

Intra-CSF AAV9 and AAVrh10 Administration in Nonhuman Primates: Promising Routes and Vectors for Which Neurological Diseases?

Karim Bey,¹ Johan Deniaud,¹ Laurence Dubreil,¹ Béatrice Joussemet,² Joseph Cristini,³ Carine Ciron,¹ Juliette Hordeaux,¹ Morwenn Le Boulc'h,¹ Kevin Marche,¹ Maud Maquigneau,² Michaël Guilbaud,² Rosalie Moreau,¹ Thibaut Larcher,¹ Jack-Yves Deschamps,¹ Marion Fusellier,⁴ Véronique Blouin,² Caroline Sevin,^{5,6} Nathalie Cartier,⁶ Oumeya Adjali,² Patrick Aubourg,^{5,7} Philippe Moullier,² and Marie-Anne Colle¹

¹UMR PANTher 703 INRA/Oniris Animal Pathophysiology and Bio Therapy for Muscle and Nervous System Diseases, Oniris, Nantes-Atlantic College of Veterinary Medicine Food Sciences and Engineering, 44307 Nantes Cedex 03, France; ²INSERM, UMR1089, Translational Gene Therapy for Genetic Diseases, Nantes, France; ³Department of Neurosurgery, Nantes Hospital, Nantes, France; ⁴Department of Medical Imaging, Oniris, Nantes-Atlantic College of Veterinary Medicine Food Sciences and Engineering, 44307 Nantes Cedex 03, France; ⁵Service de Neuropédiatrie, Hôpital Bicêtre-Paris Sud, 78 rue du Général Leclerc, 94275 Le Kremlin-Bicêtre Cedex, France; ⁶INSERM U1127, Institut du Cerveau et de la Moelle épinière (ICM), Hôpital Pitié-Salpêtrière, 47 boulevard de l'hôpital, 75013 Paris, France; ⁷INSERM U1169, Thérapie Génique, Génétique, Epigénétique en Neurologie, Endocrinologie et Développement de l'Enfant, Université Paris Sud, CEA, Le Kremlin Bicêtre, France

The identification of the most efficient method for whole central nervous system targeting that is translatable to humans and the safest route of adeno-associated virus (AAV) administration is a major concern for future applications in clinics. Additionally, as many AAV serotypes were identified for gene introduction into the brain and the spinal cord, another key to human gene-therapy success is to determine the most efficient serotype. In this study, we compared lumbar intrathecal administration through catheter implantation and intracerebroventricular administration in the cynomolgus macaque. We also evaluated and compared two AAV serotypes that are currently used in clinical trials: AAV9 and AAVrh10. We demonstrated that AAV9 lumbar intrathecal delivery using a catheter achieved consistent transgene expression in the motor neurons of the spinal cord and in the neurons/glia cells of several brain regions, whereas AAV9 intracerebroventricular delivery led to a consistent transgene expression in the brain. In contrast, AAVrh10 lumbar intrathecal delivery led to rare motor neuron targeting. Finally, we found that AAV9 efficiently targets respiratory and skeletal muscles after injection into the cerebrospinal fluid (CSF), which represents an outstanding new property that can be useful for the treatment of diseases affecting both the central nervous system and muscle.

INTRODUCTION

Neurodegenerative disorders are a major challenge for medicine and public health due to demographic changes worldwide. The adeno-associated virus (AAV) vector, as a nonpathogenic viral particle, represents a powerful and promising therapeutic approach for human neurological diseases. As a result, several clinical trials applied to several human neurological genetic disorders (Sanfilippo type A

and B, ClinicalTrials.gov: NCT02053064 and NCT03300453, respectively; Batten disease, ClinicalTrials.gov: NCT01414985; metachromatic leukodystrophy, ClinicalTrials.gov: NCT01801709; and spinal muscular atrophy, ClinicalTrials.gov: NCT02122952) were initiated by using AAVs. Direct brain parenchymal and intravenous deliveries are commonly used in clinical trials. In mice and large animal models, AAV9 was able to bypass the blood-brain barrier (BBB) and target predominantly neurons and spinal motor neurons (MNs), especially when the vector was administered intravenously at an early stage of life.^{1,2} These AAV9 properties show spectacular outcomes in animal models^{3,4} and clinically⁵ in the context of spinal muscular atrophy (SMA), which is a devastating MN disease. However, the translational feasibility of intravascular AAV administration is limited by the following: (1) the high doses required to achieve efficient vector diffusion and transgene expression in the CNS, which could lead to a potential off-target-based toxicity immunological response, and (2) the required challenging manufacturing process.^{6–8} Local intraparenchymal delivery overcomes the BBB. Indeed, efficient and long-term gene transfer in many brain structures has been described in several animal models after the intraparenchymal injection of the AAV vector in a restricted brain-injected region, such as in Parkinson's disease,^{9–13} or after multiple injection tracks in the brain, such as in lysosomal storage disease or more specifically, leukodystrophy.^{14–17} Several clinical trials have confirmed the high potential of this route of administration, with excellent safety and encouraging results in human patients for these applications.^{18,19} However, intraparenchymal injection leads to a limited diffusion of

Received 10 March 2020; accepted 2 April 2020;
<https://doi.org/10.1016/j.omtm.2020.04.001>

Correspondence: Marie-Anne Colle, INRA/Oniris UMR 703, Oniris, Route de Gachet, CS 40706, F-44307 Nantes, France.

E-mail: marie-anne.colle@oniris-nantes.fr



the AAV vector, mainly in cells surrounding the injection site.²⁰ Thus, this approach is difficult to apply in neurodegenerative diseases in which global CNS transduction in the brain and spinal cord is required.

In parallel, many research groups are developing cerebrospinal fluid (CSF)-based delivery via intracerebroventricular (ICV) injection, *cisterna magna* administration (ICM), or lumbar intrathecal puncture (LIT). These studies have successfully demonstrated that CSF administration of AAV is efficient to deliver genes into cells throughout the brain and in the entire spinal cord in rodents, cats, dogs, and nonhuman primates (NHPs).^{21–25} Among all serotypes tested, AAV9 and AAVrh10 show the highest neurotropism following intra-CSF delivery.^{26,27} These promising results open up the field of gene therapy to numerous neurodegenerative diseases, giving a renewed hope to find a cure. However, the vast majority of the encouraging results in the preclinical model were obtained after administration of the therapeutic vector into the *cisterna magna*.^{28–30} Although this procedure is common and safe in veterinary medicine, it is highly risky in humans due to the proximity of vital brainstem centers. Due to this high-risk factor, ICM administration represents a nonprivileged method for the delivery of potential AAV medicine products in human trials.

To develop a translational therapeutic approach for human neurodegenerative diseases, we designed neurosurgical procedures in close collaboration with neurosurgeons. In the present study, we aimed to determine the most efficient and safe intra-CSF delivery for optimal gene transfer in an NHP model. Both tested approaches of administration, ICV and lumbar intrathecal puncture using a transitory catheter (LIT-KT), have previously been approved and performed in human clinics. As a second aim, we determined the most efficient serotype, between AAV9 and AAVrh10, to target and induce transgene expression in neuronal and glial cells across the entire CNS. We also assessed other variables critical for a translational approach, including biodistribution to peripheral organs and immunogenicity induced by the CSF delivery of AAV vectors.

RESULTS

Clinical Outcomes Following Intra-CSF Surgical Procedures

To demonstrate the safety and reproducibility of both ICV and LIT-KT deliveries, the study was initiated with a significant set of animals ($n = 2$ and 4 , respectively) using a contrast agent solution to monitor catheter positioning, control diffusion through the CNS, and monitor the intracranial pressure (ICP) to avoid intracranial hypertension.

Several studies, including ours, have demonstrated efficient transgene expression throughout the spinal cord after AAV9 delivery in the *cisterna magna* of rodents, cats, and NHPs.^{28–32} Suboccipital puncture is commonly used in veterinary medicine but is only rarely performed in humans, due to the high risk of encountering vessels during the procedure and the risk of hemorrhagic or ischemic complications. Therefore, we targeted the lateral ventricles, which have

the advantage of being close to *cisterna magna* with a safer approach. A pilot study was first performed in 2 NHPs to set up the ICV surgical procedure. The correct placement in the lateral ventricle was verified under real-time radioscopic examination (Figure 1A). Contrast solution was visualized, showing a lateral ventricle that retained a radio-opaque solution, as demonstrated by yellow arrowheads (Figure 1A1). 10 s after administration, contrast agent was observed in the cervical (Figure 1A1), thoracic (Figure 1A2), and lumbar spinal cord (Figure 1A3) areas. Real-time video radioscopy was performed to illustrate the flow of contrast agent from the lateral ventricle to the cervical spinal cord (Video S1). To limit CSF leakage from the injection site and therefore AAV vector leakage after lumbar puncture and to promote homogeneous distribution along the spinal cord, we optimized the surgical procedure by implementing LIT-KT. Intraspinal catheters have been used routinely for decades in various surgical and anesthesia settings.³³ We used the same intrathecal catheter as used in pediatric medicine, and we introduced this catheter with an atraumatic SPOTTE cannula³⁴ (Figure 1B3, inset). Under radioscopic control, the catheter was advanced until its tip was situated at the level of the last cervical vertebrae. We performed 3 deposits of 1 mL of PBS-contrast solution at the cervical thoracic and the lumbar level. A positive signal at radioscopy demonstrates the spreading of the solution into the *cisterna magna*, along the cervical spinal cord (Figure 1B1) and the thoracic spinal cord (Figure 1B2), as demonstrated by white arrowheads, and along the lumbar spinal cord (Figure 1B3). To determine whether intra-CSF administration was associated with ICP and to assess this safety aspect, we monitored intracranial pressure throughout the ICV and LIT-KT infusion in all NHPs (Figure 1C). The normal range for intracranial pressure is below 20 mmHg; above this limit, increased ICP occurs and may lead to potentially devastating CNS injuries.³⁵ For the pressure monitoring of ICV administration, we injected NHP-01 and NHP-02 with 2.5 and 1 mL, respectively, with PBS-contrast agent solution. For NHP-01, the needle was inserted into the right lateral ventricle, and CSF pressure was measured at 9 mmHg. Then, 1.5 mL of PBS was injected, leading to 16 mmHg. Finally, an additional 1 mL of PBS was injected, leading to a CSF pressure of 21 mmHg. To determine whether intracranial hypertension is a transitory phenomenon, we measured the CSF pressure at 15 min post-injection and observed a restoration of the CSF pressure to 17 mmHg. For NHP-02, we removed approximately 1 mL of CSF by using spinal tap. Subsequent pressure measurements following CSF tap indicated a CSF pressure of 16 mmHg. Then, 1 mL of PBS was injected with a 0.1-mL step. CSF pressure was measured after the injection of 0.2, 0.3, 0.5, 0.7, and 1 mL of solution, leading to 17, 18, 20, 22, and 23 mmHg, respectively. Finally, at 15 min postadministration, we observed a decrease in CSF pressure to 17 mmHg.

For LIT-KT pressure monitoring, NHP-03, -04, -05, and -06 were injected with 3 mL of PBS. All NHPs were subjected to CSF tap (approximately 1 mL), and CSF pressure measurements indicated a range of 5–6 mmHg for all NHPs. The CSF pressure assessment before spinal tap (performed in NHP-03 and NHP-06) indicated 13 and 10 mmHg, respectively, demonstrating the effect of spinal

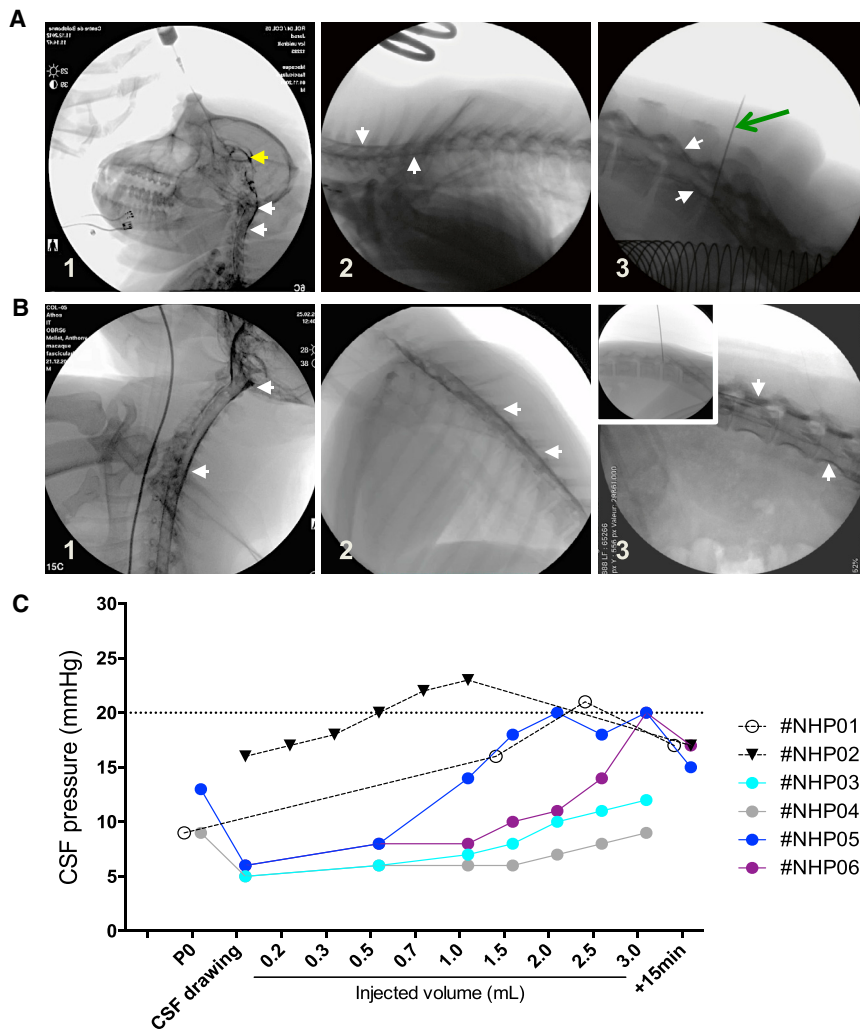


Figure 1. Procedure, Contrast Agent Diffusion, and CSF Pressure Monitoring of the LIT-KT and ICV Administration in NHP

(A) Placement of the needle into the right lateral ventricle was confirmed by fluoroscopic imaging and free-flowing cerebrospinal fluid. A representative image of contrast solution distribution into the right lateral ventricle (yellow arrow) at the time of intracerebroventricular injection and into the cervical spinal cord (A1) and 10 s after contrast solution administration into the thoracic (A2) and lumbar (A3) spinal cord. (B) Lumbar intrathecal puncture and SPROTTE cannula placement was performed into the lumbar intrathecal subarachnoid space of NHP. Fluoroscopic imaging and free-flowing CSF confirmed the position of the cannula (B3, inset). Then, the catheter was ascended to the cervical vertebrae under fluoroscopic monitoring, and 1 mL of contrast solution was injected (B1). The same procedure was performed for thoracic (B2) and lumbar contrast solution deposits (B3). White arrows indicate the signal from the contrast solution, and the green arrow indicates the needle used for CSF pressure monitoring. (C) Contrast solution was injected in NHPs following IT (n = 4; #NHP-01–#NHP-04) or ICV (n = 2; #NHP-05 and #NHP-06) administration, and the ICP was monitored in accordance with the intrathecal-injected volume. For LIT-KT-injected NHPs, ICP was monitored at the cannula placement (P0). Then, approximately 1 mL of CSF was removed for each NHP, and ICP was measured at the CSF drawing time point. Finally, ICP was analyzed at 0.5, 1, 1.5, 2, 2.5, and 3 mL of injected volume. An ultimate ICP measurement was performed 15 min after the end of contrast solution administration (+15 min time point). For ICV administration, #NHP-05 received 0.5 mL of PBS, and ICP was measured after CSF drawing and just after contrast injection. #NHP-06 received 2.5 mL of contrast solution, and ICP was analyzed at CSF drawing, 1.5 and 2.5 mL of injected volume, and 15 min after injection. Finally, #NHP-07 received 1 mL of contrast solution, and ICP was monitored at CSF drawing, 0.2, 0.3, 0.5, 0.7, and 1 mL of injected volume, and 15 min after administration.

tap on CSF pressure. Then, CSF pressure was analyzed after the injection of 0.5, 1, 1.5, 2, 2.5, and 3 mL of PBS. The measurements in all NHPs indicated a constant increase in CSF pressure. It is important to mention that measurements not exceeding 20 mmHg, following IT administration, indicate no intracranial hypertension. Finally, measurements in NHP-05 and NHP-06 (animals that reached 20 mmHg, the highest point observed following LIT-KT injection of 3 mL of PBS) at 15 min postadministration demonstrated the decrease and restoration of CSF pressure. Based on this pilot experiment, we removed 1 mL of CSF and injected 0.5 and 3 mL through ICV and LIT-KT, respectively, for the following intra-CSF AAV administration experiments in NHPs. The magnetic resonance imaging (MRI) follow-up on the day of injection and at 3 days and 21 days post-injection did not show any abnormality (data not shown), as confirmed by neurobehavioral examination, which confirmed the safety profile of our ICV and LIT-KT administration approaches.

AAV9 Achieved Strong MNs and Consistent Brain Transduction Compared to the AAVrh10 Serotype

We designed an experiment to compare the pattern of transgene expression in the NHP CNS following LIT-KT injection of both AAVrh10 (n = 2) and AAV9 (n = 4) expressing green fluorescent protein (GFP) (Table 1). A total of 2.5E+13 vector genomes (vg) in 3 mL of vector solution was injected into NHPs by the LIT-KT route of injection. For the group injected using AAVrh10-chicken β-actin promoter with cytomegalovirus enhancer (CBA)-GFP, no cell bodies expressed the GFP protein in the lumbar segment of the spinal cord. Only fibers expressing the GFP protein were found specifically in the dorsal horns (Figure 2A). In the thoracic segment, cell bodies and fibers expressed the GFP transgene, and at the cervical level, rare MNs showed GFP-positive signals (Figure 2A). Analysis of the animals injected with AAV9-CBA-GFP revealed strong GFP expression localized to ventral horns at all levels of the spinal cord (Figure 2A). Higher magnification in

Table 1. Summary of Experimental Design

Animal Identification	Age (Years)	Weight (kg)	Gender	Route	Capsid	Dose (vg)	Volume (mL)
Mac 1	3	3	M	LIT-KT	10	2.50E+13	3
Mac 2	3	3.1	M	LIT-KT	10	2.50E+13	3
Mac 3	3	3.4	M	LIT-KT	9	2.50E+13	3
Mac 4	2.5	3.1	M	LIT-KT	9	2.50E+13	3
Mac 5	3	3.7	M	LIT-KT	9	2.50E+13	3
Mac 6	2.5	3.4	M	LIT-KT	9	2.50E+13	3
Mac 7	2	3.2	M	ICV	9	4.50E+12	0.5
Mac 8	2	2.7	M	ICV	9	4.50E+12	0.5

M, male; LIT-KT, lumbar intrathecal puncture using a transitory catheter; ICV, intracerebroventricular.

the ventral horns of cervical, thoracic, and lumbar spinal cord transversal sections revealed specific and robust GFP expression in MNs (Figure 2A). Interestingly, longitudinal sections demonstrated an abundance of MNs expressing GFP throughout 5 mm of tissue (Figures S1A and S1B; Figure 3A, lower magnification). To identify the cell type expressing GFP in ventral horns, we performed immunofluorescence staining using ChAT, GFAP, Olig2, and Iba1 for MNs, astrocytes, oligodendrocytes, and microglial cells, respectively, in AAV9- and AAVrh10-injected NHPs. This experiment revealed the specific colocalization of GFP protein in MNs (Figure 3A). No GFP signal was observed in glial cells (Figure S2). The quantification of MNs expressing GFP by using ChAT immunofluorescence was performed after checking the specificity of the GFP (Figures S3A–S3C). GFP-positive MN quantification revealed 0.26% to 0.31% in the cervical segment, 0% in the thoracic segment, and 0% to 0.31% in the lumbar segment of the spinal cord for self-complementary (sc) AAVrh10-injected animals and 3.39% to 44.75% at the cervical level, 1.31% to 59.5% at the thoracic level, and 5.45% to 66.26% at the lumbar level of the spinal cord for AAV9-injected NHPs (Figure S3D). Since AAV9 seems to be the better serotype to target neuronal cells, we introduced a third group of injected NHPs (n = 2) using ICV administration to compare both the LIT-KT and ICV routes of injection in a large animal model. The volume of injection into the ventricle was smaller for safety consideration (0.5 mL of vector solution), leading to a dose of 4.5E+12 vg for each AAV9-CBA-GFP ICV-injected NHP (Table 1). 3 weeks after dosing, the animals were euthanized, and confocal fluorescence imaging analysis demonstrated the strong expression and localization of GFP at all levels of the spinal cord, especially in the ventral horns (Figure 2A). Quantification revealed a percentage of MNs expressing GFP of 3.3% to 20.1% in the cervical segment, 17.35% to 19.9% in the thoracic segment, and 16.65% to 65.45% in the lumbar segment of the spinal cord (Figure S3D).

Next, we determined the brain GFP expression pattern following LIT-KT AAVrh10 or AAV9 injection. For the AAVrh10 serotype, no GFP was found in any of the brain sections. Concerning the

AAV9 serotype, patchy GFP expression was observed in several cell types across multiple regions. Analysis of GFP expression throughout several brain regions of the NHPs showed clustered transduced neuronal and glial cells in the frontal, parietal, and temporal cortices (Figure 2B). Immunofluorescence staining using neuronal and glial markers confirmed the presence of GFP-positive neurons, oligodendrocytes (in white matter), and astrocytes, whereas no microglial cells expressed GFP (Figure 3B). Deeper brain regions were analyzed. Rare neurons and astrocytes expressed GFP in the hippocampus (Figure 2B), putamen, hypothalamus, and body of caudate nucleus (Figure S4). In the cerebellum, GFP was mainly expressed in white matter oligodendrocytes and rare neurons in the granular layer, and Purkinje cells were positive for the fluorescent protein (Figure S4).

For NHPs injected with the AAV9-CBA-GFP vector using ICV administration, we found consistent GFP expression in the frontal lobe with a high number of GFP-positive neurons (Figure 2B). In the parietal and temporal cortices, the pattern of GFP expression was similar to that of LIT-KT-injected animals, with GFP-positive neurons and astrocytes (Figure 2B). Concerning the hippocampus, more neurons and glial cells expressed GFP. The GFP distribution and expression were similar to that observed in the cerebellum of LIT-KT-injected animals (Figure 2B); however, consistent glial GFP expression was observed close to the 4th ventricle (Figure S4). Finally, we found a similar pattern of GFP distribution in the hypothalamus, and rare neuronal and glial cells expressed GFP in the dorsolateral geniculate nucleus of the thalamus (Figure S4).

The AAVrh10 Serotype Leads to Specific and Robust GFP Expression in Dorsal Root Ganglia (DRG) Neurons

Following the consistent transduction achieved in the spinal MN of NHPs injected with the AAV9 serotype, we investigated whether AAVrh10 and AAV9 serotypes were able to transduce the peripheral nervous system, more specifically, DRG. Following LIT-KT AAVrh10 and AAV9, the majority of DRG expressing GFP was found at the cervical and lumbar levels. Thoracic DRG were less transduced. We found robust GFP expression in the

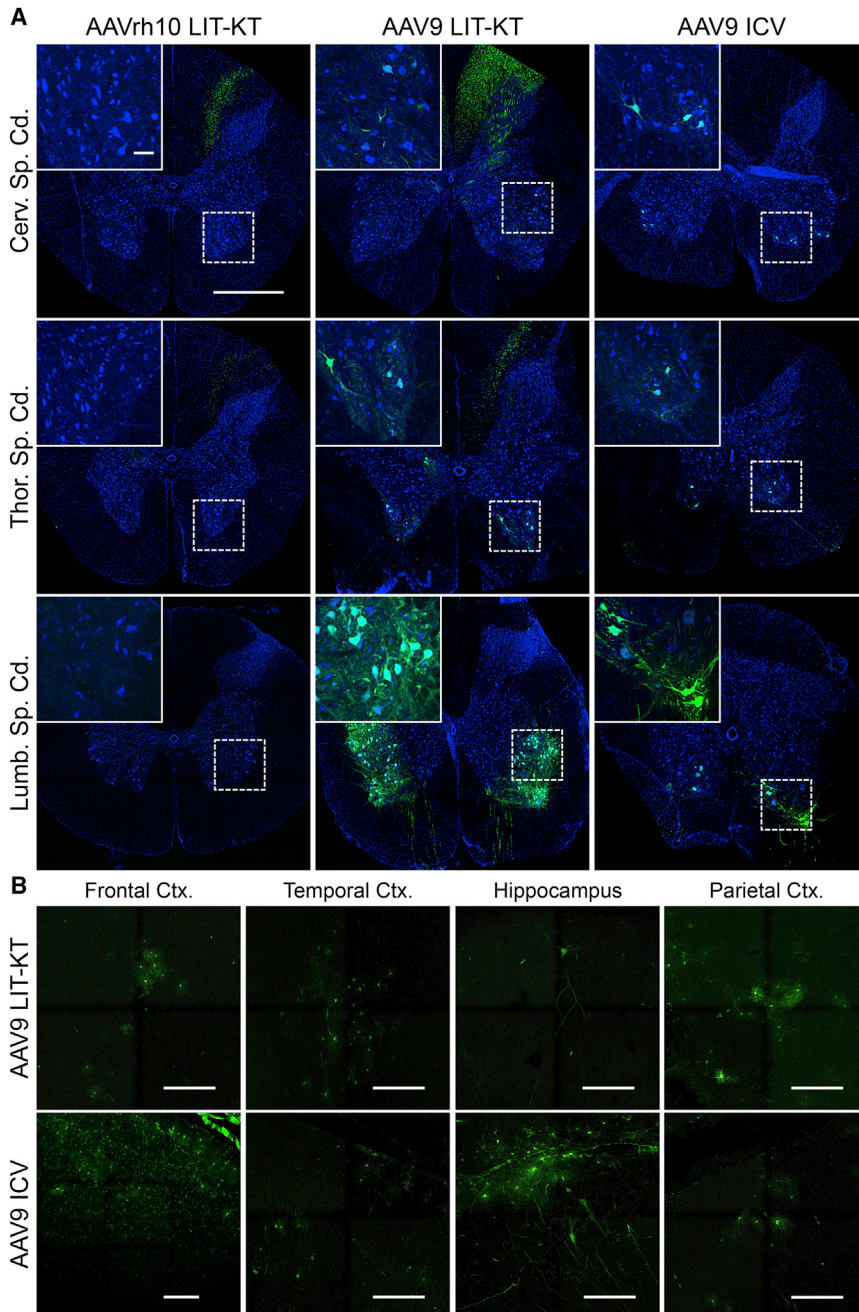


Figure 2. Effect of the Route of Administration and AAV Serotype on the GFP-Transgene Expression Profile

(A) Spinal cord transduction following LIT-KT injection of the AAVrh10 and AAV9 serotypes or following AAV9 ICV injection. The representative whole spinal cord transverse section indicates rare/no transduction of the ventral horn gray matter for NHPs injected with AAVrh10, whereas transduction is observed primarily in the ventral horn for NHPs injected with LIT-KT and ICV AAV9. Green fluorescence illustrates the native GFP-positive signal and blue the nuclear 4',6-diamidino-2-phenylindole (DAPI) signal. Hatched windows indicate regions of interest (ROIs) presented in the insets that show higher magnification of the ROI. Main image scale bar, 1 mm; inset scale bar, 100 μ m. (B) Representative transduction throughout several brain regions following LIT-KT and ICV AAV9 administration. The green fluorescence signal illustrates the native GFP-positive signal. Scale bars, 150 μ m.

peptide derived from preprotachinin. Involvement of SP in nociception and chronic pain syndrome is well established.³⁶ SP immunostaining did not reveal any colocalization with GFP in the cervical and lumbar DRG for either AAV serotype (Figure 4B). These results suggest that AAVrh10 and AAV9 do not preferentially target sensitive neurons secreting SP. Finally, recent studies showed that systemic or *cisterna magna* AAV9 injection in NHP models triggered robust and mild axonal and neuronal degeneration, respectively, in DRG, characterized by cluster of differentiation (CD)3 T cells and mononuclear cells infiltrates.^{37,38} Additionally, mice injected with AAV9-GFP by lumbar puncture displayed mononuclear aggregates and infiltrates and multifocal neuronal necrosis and loss in DRG.³⁹ We therefore focused our attention on this safety aspect. Subsequent histopathological examination revealed multifocal mild mononuclear cell infiltration in thoracic and lumbar DRG for LIT-KT AAVrh10-injected Mac 1 and Mac 2 animals,

soma of large-diameter neurons, mainly, and in fibers within all transduced DRG (Figure 4A). For AAV9 ICV-injected NHPs, the majority of DRG expressing GFP protein was observed distally to the injection site in thoracic and lumbar segments with a high number of GFP-positive, large-diameter neurons and some fibers (Figure 4A). Rare but GFP-positive, large-diameter neurons were found at the cervical site (Figure 4A). To characterize the type of sensory neurons transduced in DRG, we performed immunofluorescence staining against the substance P (SP) marker, a neuro-

respectively (Figure S5). The same observations were found in LIT-KT AAV9-injected monkeys at the lumbar DRG site for Mac 4 and Mac 6 animals (Figure S5). Moderate mononuclear cell infiltration was observed in cervical and lumbar DRG for Mac 3 animals (Figure S5). Moreover, in DRG fibers from Mac 4, Mac 5, and Mac 6 animals, we also found mononuclear cell infiltration and digestion chambers that lead to myelin degradation (Figure S5). Histopathological examination of the brain did not reveal any lesions.

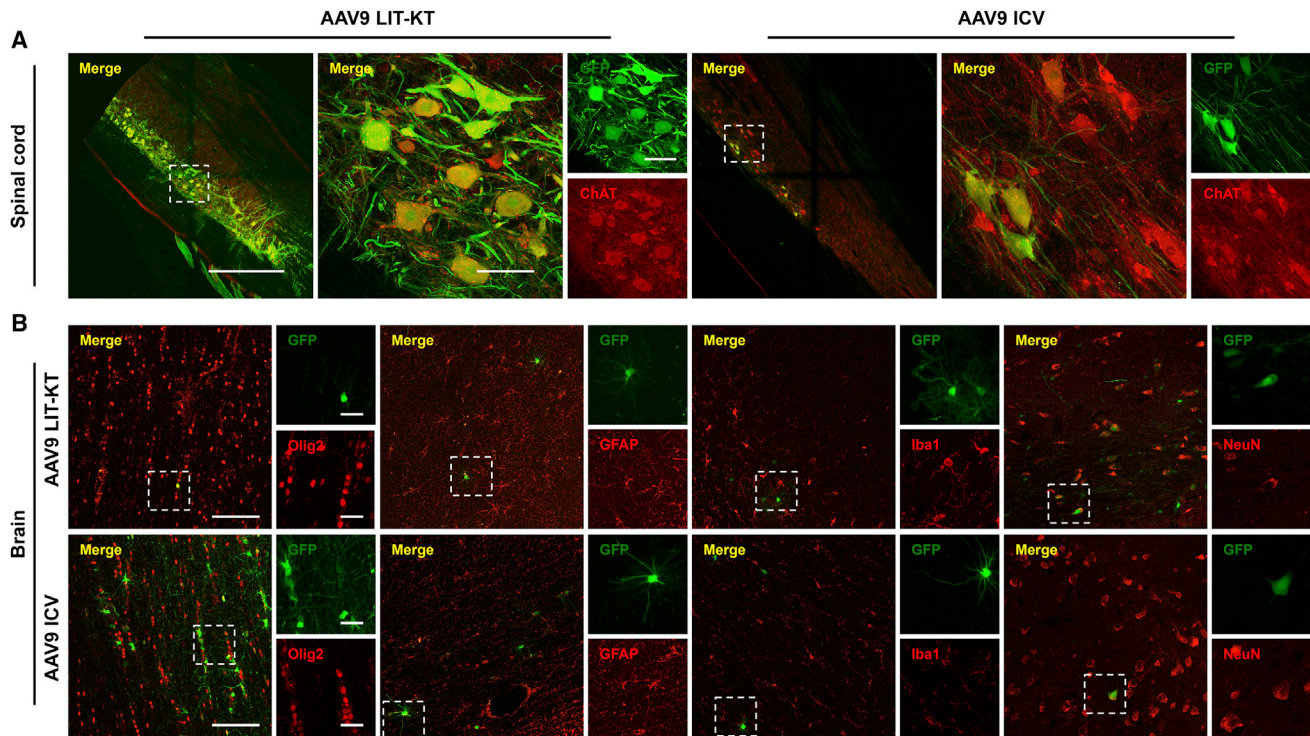


Figure 3. Transduced Cell-Type Identification Throughout the Brain and Spinal Cord Following AAV9 Intra-CSF Delivery

(A) AAV9 motor neuronal tropism was determined using ChAT (red channel) immunostaining in lumbar and thoracic spinal cord from NHPs injected by LIT-KT or ICV, respectively. Main images show Alexa 555/GFP merged fluorescence signals. Scale bars, 1 mm (left) and 100 μ m (right). Insets show higher magnification on neurons harboring both fluorescence signals: GFP (top) and Alexa 555 (bottom) channels. Scale bar, 100 μ m. (B) AAV9 cell-specific tropism was determined in brain representative sections from NHPs injected by LIT-KT and ICV. Brain tissues were immunolabeled using Olig2, GFAP, Iba1, and NeuN primaries for oligodendrocytes, astrocytes, microglial cells, and neuron phenotyping, respectively, and an Alexa 555 (red channel)-coupled secondary antibody was used for cell detection. GFP was determined by native GFP fluorescence signal imaging (green channel). Main images show Alexa 555/GFP merged fluorescence signals. Scale bars, 100 μ m. Hatched windows indicate regions with GFP-positive cells, and insets show higher magnification on cells harboring both fluorescence signals: GFP (top) and Alexa 555 (bottom) channels. Scale bars, 25 μ m.

Intra-CSF AAV Administration Achieves Broad GFP Expression in the Skeletal and Respiratory Muscles and Heart and Moderate GFP Expression in the Liver

To determine whether intra-CSF delivery leads to peripheral organ targeting, we examined several anatomically distinct skeletal and respiratory muscles, the heart, and the liver of all NHPs included in this study. Diaphragm, gastrocnemius, and triceps brachii muscles were collected to compare and quantify GFP expression in muscle fibers. Interestingly, we found a high number of diaphragmatic muscle fibers expressing GFP protein following LIT-KT injection of both serotypes (Figure 5A). However, quantification revealed a higher number of GFP-expressing diaphragmatic muscle fibers with the AAV9 serotype ($\approx 54.2\%$ of total fibers) than with the AAVrh10 serotype ($\approx 33.3\%$ of total fibers) (Figure 5B). Surprisingly, ICV administration of scAAV9-CBA-GFP achieved diaphragm muscle transduction (Figure 5A), but a lower amount, approximately 15% of total fibers, was transduced (Figure 5B). Analysis of the gastrocnemius muscle demonstrated a higher percentage of transduced fibers for AAV9 LIT-KT ($\approx 36.5\%$) and AAV9 ICV ($\approx 32.2\%$) than for AAVrh10 LIT-KT, which led to approximately 22.7% of transduced muscle fi-

bers (Figures 5A and 5B). Concerning the triceps brachii muscle, the AAVrh10 serotype achieved a higher percentage of fiber transduction than did the AAV9 serotype ($\approx 33.3\%$ and 19.7%, respectively). Only 1/4 of the AAV9 LIT-KT-injected NHPs reached 38.9% of transduced muscle fibers of the triceps brachii. AAV9 ICV administration led to limited muscle fiber transduction, since approximately 2.7% of total muscle fibers were GFP positive (Figure 5B). Cardiac tissue analysis demonstrated moderate GFP expression by using LIT-KT AAV9 administration, whereas LIT-KT AAVrh10 and ICV AAV9 led to poor GFP expression (Figures 5A and 5C). Finally, analysis of the liver demonstrated an equivalent proportion of GFP expression throughout all groups (Figures 5A and 5C). Regarding the limited number of animals used in this study, it was not possible to make a direct correlation between the serotype and/or the route of administration and the muscle fibers, heart, and liver transgene expression. Finally, we performed a qualitative analysis of peripheral organs in all AAV-injected groups. The fluorescence analysis by confocal microscopy revealed GFP expression into the thymus, spleen, kidney, jejunum, and testis; however, no GFP transgene was observed into the lung in all AAV-injected groups (Figure 5G). Taken

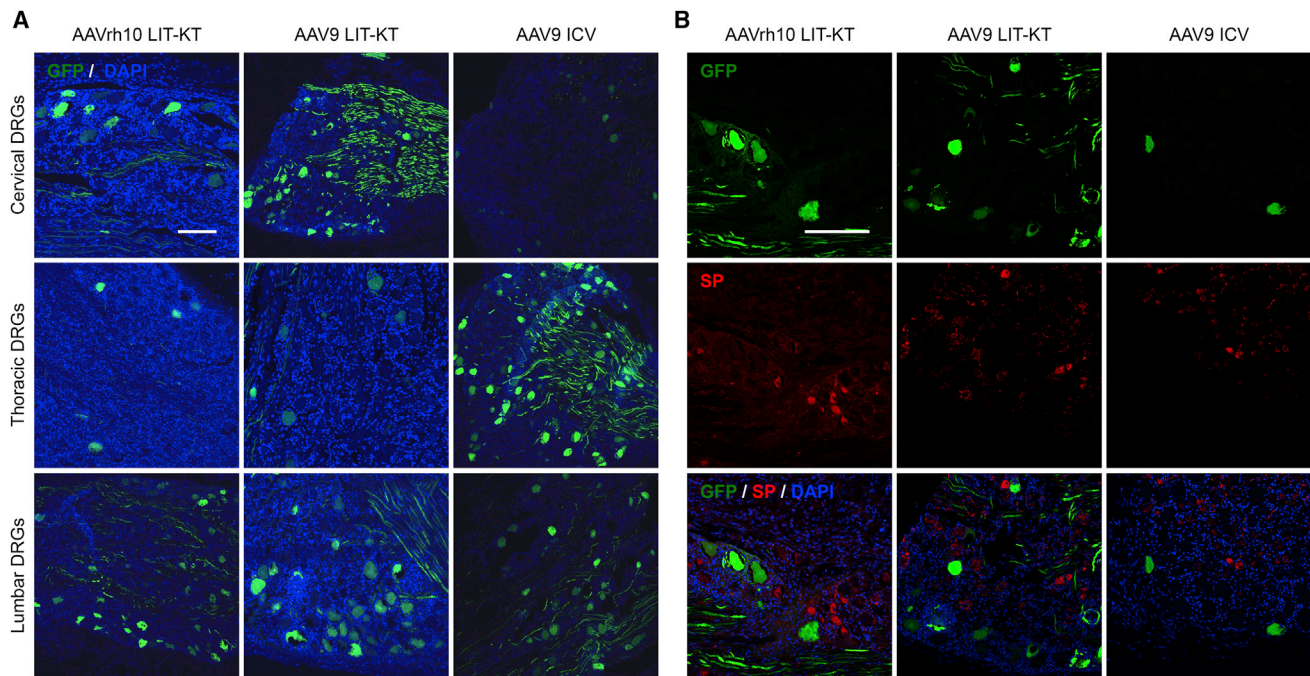


Figure 4. GFP-Transgene Expression into the Peripheral Nervous System after Intra-CSF AAV9 or AAVrh10 Administration

(A) Representative images demonstrate the native GFP fluorescence signal analyzed using confocal imaging in the cervical, thoracic, and lumbar DRG from NHPs injected with AAVrh10 and AAV9 by LIT-KT and AAV9 by ICV route of administration. DAPI was used for nuclear counterstaining. Scale bar, 200 μm . (B) SP immunostaining was performed in thoracic and lumbar DRG and revealed using an Alexa 555 (red channel) secondary antibody. The green channel displays the native GFP fluorescence. Cervical DRGs are not presented in this figure. Scale bar, 150 μm .

together, these results suggested a consistent escape of AAV particles from the CSF to peripheral organs after intra-CSF administration that allowed transgene expression in NHPs.

Escape of AAV Particles from the CNS to the Peripheral Compartment Is a Rapid Phenomenon Mediated by Blood Circulation

Since AAV9 and AAVrh10 allowed transgene expression in peripheral organs, we focused our attention on the AAV distribution throughout CSF and serum over a 24-h period to determine the dynamics of viral particles following intra-CSF administration. NHPs injected by AAVrh10 LIT-KT, AAV9 LIT-KT, and AAV9 ICV were subjected to blood and CSF drawing after AAV dosing. As a baseline control, viral particle detection was performed before AAV dosing in both fluids. Analysis of the CSF revealed rare detection of viral particles at 7 and 19 days following dosing in all injected NHPs in this study (Figure 6A). Serum analysis demonstrated the presence of viral particles at 1 h following dosing (day 0 [D0] +1 h), which represented an average of approximately 4.85%, 6.99%, and 4.58% of the total injected dose for AAVrh10 LIT-KT, AAV9 LIT-KT, and AAV9 ICV, respectively. It is important to note that this time point was higher in terms of concentration in peripheral blood, since we found 1.62%, 5.07%, and 1.30% of the total injected dose for AAVrh10 LIT-KT, AAV9 LIT-KT, and AAV9 ICV, respectively, at 3 days postdosing (Figure 6B). Finally, at 7, 10, and 19 days

post-injection, the AAV serum concentration was approximately zero (Figure 6B). These results suggest a rapid distribution to peripheral organs of AAV viral particles after intra-CSF dosing.

Since we demonstrated the presence of circulating AAV in the bloodstream, we examined whether AAV particles injected by the intra-CSF route could trigger a peripheral immune response against the serotype capsid and GFP transgene. To this end, serum and CSF samples were analyzed for the prevalence of neutralizing factors (NFs) against both serotypes used in this study. We also evaluated whether NF formation was dependent on the route of injection. Baseline serum samples revealed an NF titer less than 1/10 for all NHPs, except Mac 6, which displayed a titer of 1/100. At 3 days post-AAV administration, all animals presented an NF titer less than 1/10; however, 5/6 AAV9-injected animals showed a significant increase ($\geq 1/1,000$) in the NF serum titer at 1 week post-injection. At 10 days post-CSF dosing and at sacrifice, all animals in this study were significantly positive for NF in the serum (Table 2). Interestingly, evaluation of the NF titer in the CSF revealed no change compared to baseline in 5/8 NHPs; however, 3/8 animals displayed a 1/100 neutralizing antibody (NAb) titer in CSF (Table 2). Concerning the GFP transgene, lymphocyte T CD8⁺ response monitoring by interferon gamma ELISpot detection demonstrated a cellular immune response against the GFP protein for Mac 1, Mac 3, and Mac 4 animals (Table S1). Quantification of the titer of antibodies against GFP in serum revealed an increase in

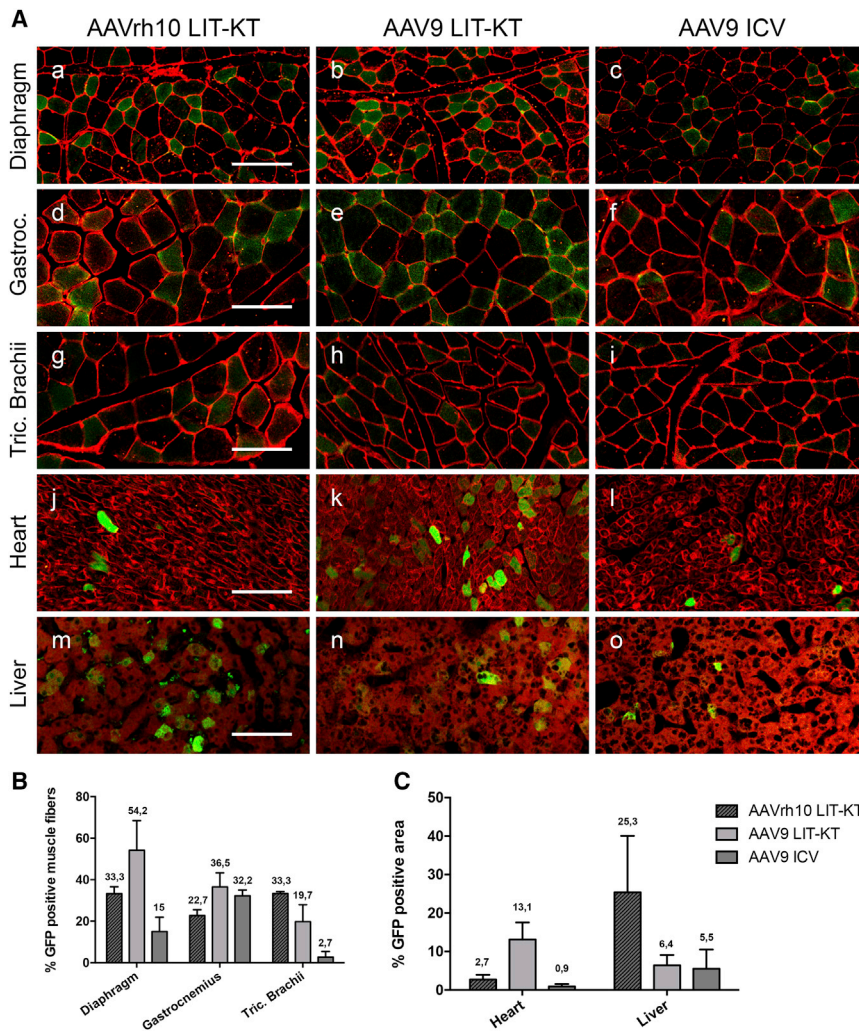


Figure 5. Muscle and Peripheral Organs Targeting Following Intra-CSF AAV9 and AAVrh10

(A) GFP expression profiles in NHP diaphragm, gastrocnemius, triceps brachii muscles, heart, and liver following AAVrh10-CBA-GFP LIT-KT delivery and AAV9-CBA-GFP administration via LIT-KT and ICV routes. (a–l) GFP fluorescence, green; wheat germ agglutinin (WGA)-Alexa 555 fluorescent labeling, red. Scale bars, 50 μ m. (Am–o) GFP fluorescence, green; unmixed autofluorescence, red. Scale bar, 25 μ m. (B) % GFP-positive muscle fibers quantified from diaphragm, gastrocnemius, and triceps brachii muscle sections of NHPs injected with AAVrh10-CBA-GFP LIT-KT ($n = 2$) and of NHPs injected with AAV9-CBA-GFP administration via the LIT-KT route ($n = 4$) and ICV delivery ($n = 2$). Data represented on the graph corresponded to at least 1,000 muscle fibers. (C) % GFP-positive area quantified from heart and liver sections of NHPs injected with AAVrh10-CBA-GFP LIT-KT delivery ($n = 2$) and of NHPs injected with AAV9-CBA-GFP administration via LIT-KT ($n = 4$) and ICV routes ($n = 2$). Data represented on the graph corresponded to at least 2 mm^2 of tissue area investigated, with approximately 1,000 cells explored.

terial used in the human clinic, we demonstrated that injection into the lateral ventricle of NHPs was well tolerated. No adverse event was reported in clinical-outcome monitoring assessed by global activities, fine motor functions, ocular activities, and attention. Safety consideration regarding CNS surgical procedure includes ICP. Since CSF homeostasis is highly sensitive, and positioning of the body or fluid injection can lead to the increase in the ICP,⁴⁰ we demonstrate robust tolerance after CSF injection of recombinant (r)AAV, sug-

gesting that both neurosurgical procedures could be translated to patients.

To date, no studies have compared AAVrh10 and AAV9 serotypes. We previously demonstrated that AAVrh10 led to moderate MN targeting compared to AAV9 by using an IT route in mice.²⁴ We also demonstrated that compared to the AAVrh10 serotype, AAV9 achieved the best molecular, histologic, and phenotypic correction of Pompe disease in the CNS of a mouse model.³⁰ Previous studies reported in a marmoset primate model that a single lumbar injection of AAVrh10-CBA-GFP, respectively, at a dose of 2.7×10^{12} vg or of 6×10^{12} vg/kg led to efficient MN transduction along the spinal cord.⁴¹ Recently, the same group reported that in *cynomolgus macaque*, lumbar intrathecal delivery of an AAVrh10-polymerase III-microRNA (miR)-GFP optimized using a catheter extended to the low thoracic region at a dose of 3.5×10^{13} vg led to profound superoxide dismutase 1 (SOD1) silencing and consistent GFP expression in MNs in the cervical, thoracic, and lumbar areas of the spinal cord and in the brain.⁴² An inferior dose (2.5×10^{13} vg per NHP) was

concentration for Mac 1, Mac 3, Mac 4, and Mac 5 animals (Table S1). Interestingly, this result was closely correlated with the cellular immune response against the GFP transgene. However, in our study, we were unable to make a correlation between the route of administration and the anti-GFP antibody titer because of the limited number of injected NHPs per group.

DISCUSSION

We and others have demonstrated the efficiency of spinal cord and brain targeting following AAV administration by using suboccipital (*cisterna magna*) or single lumbar puncture in rodents and large animal models.^{24,28,30} However, intra-*cisterna magna* delivery may not be clinically translatable, and the lumbar intrathecal route allows moderate transgene expression in the upper part of the spinal cord and in the brain.²⁴ The ICV route was previously used in a large animal model for AAV delivery into the CNS, demonstrating therapeutic benefits and a good safety profile.²⁹ However, to our knowledge, no groups have developed ICV delivery in NHPs. Under the supervision of neurosurgeons in a large animal model facility equipped with ma-

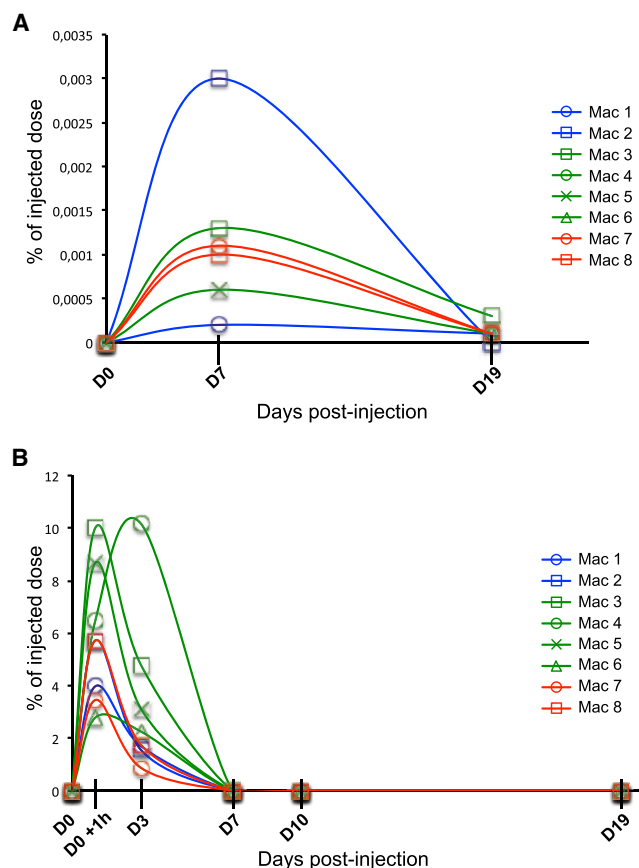


Figure 6. AAV9 and AAVrh10 Particles Shedding in the Serum and CSF

(A and B) AAV viral genome shedding was analyzed at time points 0 (before injection), 7, and 19 days after vector administration in NHPs CSF (A) and in serum at time points 0, 1 h, and 3, 7, 10 and 19 days post-injection (B). DNA viral genome increase after AAV LIT-KT and ICV injection showed the presence of AAV particles in serum and CSF and was expressed as percentage of injected total dose.

injected by LIT-KT administration in the present study. The pattern of transduction highlighted poor GFP expression in MNs along the spinal cord and no GFP expression in the brain of animals injected with AAVrh10-CBA-GFP. Several hypotheses could explain this discrepancy. First, the AAV transduction efficiency could not be the same between marmoset and *cynomolgus macaque*. Second, the vector promoter and injected dose were not the same as that used in our study design, leading to difficulties in comparing the results.⁴²

Brain transgene expression following LIT-KT injection represents an attractive strategy for the gene therapy of diseases that involve brain areas, such as Rett syndrome, Batten disease, or Pompe disease. We demonstrated that AAV9 ICV delivery allows specific GFP expression in MNs along the spinal cord; however, the percentage of transduced MNs was lower than that observed with the LIT-KT route. Regardless of the route of intra-CSF delivery, we noted that brain GFP expression was achieved mainly surrounding CD31-positive blood vessels (Figure S7), as demonstrated by other groups.^{43,44}

Our observation supports the transport of vector from CSF to the brain parenchyma through the Virchow-Robin perivascular space.^{32,45} In the brain, GFP expression mapping results are in line with previous studies that used intra-CSF delivery coupled to an AAV9-GFP vector in large animal models.^{22,23,28,29,31,46}

In the present study, intra-CSF AAV administration leads to the targeting of predominantly large-diameter neurons in DRG along the spinal cord, and this observation is in line with a previous study that demonstrated large-diameter neuronal cells mainly transduced by using AAV5 and AAV8 in a mouse model.⁴⁷ However, in our study, we did not observe substance P-positive transduced neurons into the NHP DRG, and this result is in contrast with the study of Vulchanova et al.⁴⁷ This discrepancy could be due to the animal model and the AAV serotype that they used in this study.⁴⁷ Neuronal DRG targeting following AAV9 and AAV7 ICM administration has previously been demonstrated in NHPs.³² Further investigations are needed to determine peptidergic and nonpeptidergic neuronal targeting by AAV9 and AAVrh10 following intra-CSF administration. Our study also demonstrates a particular specificity of the AAVrh10 serotype, which is to transduce mainly DRG neurons without MNs.

Another remarkable observation from our data was the ability of AAVrh10 and AAV9 serotypes to transduce skeletal and respiratory muscle fibers efficiently. We also found superior GFP expression in the heart for the AAV9 serotype following LIT-KT delivery, whereas similar GFP expression in the liver was achieved by the AAVrh10 serotype. Meyer and colleagues⁴⁶ previously reported, in a detailed biodistribution study, that both viral genome and GFP mRNA were found in diaphragm, gastrocnemius, and triceps brachii muscles. Bevan and colleagues⁶ demonstrated that intravascular AAV9-CBA-GFP, at a dose of $1E+14$ vg/kg in 1-, 30-, and 90-day-old NHPs, led to robust GFP expression in triceps brachii, diaphragm, and gastrocnemius muscles. They reported that the GFP pattern of expression in the same muscles was less abundant when the same vector was administered at a dose of $2.7E+13$ vg/kg in 3-year-old monkeys,⁶ suggesting that systemic AAV delivery requires a 3-fold dose compared to the dose used for LIT-KT AAV9 delivery in the present study; however, it is difficult to make a strong correlation because of the heterogeneity in the method of titration of AAV vector preparation. Therefore, AAV9, harboring a ubiquitous CBA promoter, coupled to LIT-KT injection, represents an attractive strategy for the treatment of neuromuscular diseases, such as SMA and amyotrophic lateral sclerosis (ALS), and lysosomal storage diseases, such as Pompe disease, since single AAV9-CBA-GFP allows robust transgene expression in the CNS, respiratory muscle, skeletal muscle, and heart. Our results, in line with Meyer and colleagues,⁴⁶ suggest peripheral AAV particle leakage from the CSF compartment to muscles and peripheral tissues. One mechanism that could explain the peripheral distribution of AAV is CSF absorption into the venous system.⁴⁸ However, another hypothesis could be considered. In fact, AAV9 can travel along neuronal axons in both retrograde and anterograde

Table 2. AAV Neutralizing Factor Titer in the Serum and CSF

Animal Identification	Route	Capsid	Serum NF Titer						CSF NF Titer	
			Baseline	d0	d3	d7	d10	dEuth	d0	dEuth
Mac 1	LIT-KT	10	<1/10	<1/10	NA	NA	NA	1/10,000	<1/10	<1/10
Mac 2	LIT-KT	10	<1/10	NA	<1/10	NA	1/10,000	1/1,000	<1/10	<1/10
Mac 3	LIT-KT	9	NA	NA	<1/10	1/1,000	1/1,000	1/10,000	NA	1/100
Mac 4	LIT-KT	9	<1/10	NA	NA	1/10,000	1/10,000	1/10,000	<1/10	1/100
Mac 5	LIT-KT	9	NA	NA	<1/10	1/1,000	1/1,000	1/1,000	<1/10	<1/10
Mac 6	LIT-KT	9	1/100	NA	<1/10	<1/10	1/1,000	1/1,000	<1/10	<1/10
Mac 7	ICV	9	<1/10	NA	<1/10	1/1,000	1/1,000	1/1,000	NA	1/100
Mac 8	ICV	9	<1/10	NA	<1/10	1/1,000	1/1,000	1/1,000	<1/10	<1/10

NF, neutralizing factor; CSF, cerebrospinal fluid; d, day; dEuth, day of euthanasia; NA, not available sample.

manners,^{49,50} and we cannot exclude AAV muscle targeting through nerve retrograde transport.

The kinetic serum shedding analysis revealed the presence of viral particles in serum at 1 h (which represented the higher concentration) and 3 days, whereas no AAV particles were detected in serum at 7 days postadministration. Additionally, we noted the superior persistence of AAV9 in the serum compared to that of AAVrh10 particles at 3 days post-LIT-KT delivery, which is in accordance with our previous study in mice.³⁰

Finally, one major aspect of AAV shedding into serum and peripheral organs that needs to be considered for clinical applications is the reaction of the immune system. All animals showed an increase in AAVrh10 and AAV9 serum NF starting on day 7, as also demonstrated by Hordeaux et al.,³⁸ following AAV9 *cisterna magna* delivery. The direct consequence of NF anti-AAV protein capsids is the impossibility of redosing animals without strong immunosuppressive treatment, specifically by using systemic injection. However, at the time of euthanasia, our results revealed a relatively low NF concentration in CSF (1/100 titer) in 3/6 injected NHPs using the AAV9 serotype. As previously demonstrated by Gray and collaborators,²² blood-circulating AAV NFs at a titer of up to 1/128 had no inhibitory effect in CNS cell transduction following intra-CSF administration of an AAV9 in NHPs.

All of these immunological arguments could lead to multiple AAV redosing in the field of human intra-CSF gene therapy, but several preclinical study needs to be performed in order to demonstrate if peripheral NFs influence CNS cell transduction following AAV intra-CSF readministration. Currently, gene therapy is promising for treating patients affected by neurodegenerative diseases. However, there is a need to support long-term therapeutic efficacy by investigation of AAV readministration, specifically for infantile neurodegenerative diseases. Lastly, the results that we obtained through this study consolidate previous findings from other groups, showing that intra-CSF administration of AAV9 may be the “gold standard” for clinical applications.

Taken together, these preclinical results support the safety and relevance of lumbar intrathecal using spinal catheter and ICV administration to deliver the AAV9 vector into the CNS and achieve efficient vector distribution and transgene expression in the brain and spinal cord. This study also provides evidence that neuron, MN, and glial cell transduction are superior with AAV9 compared to the AAVrh10 serotype. Furthermore, this study highlights that AAV intra-CSF injection represents a promising strategy for the gene therapy of neuromuscular disorders, due to this efficient respiratory and skeletal muscle targeting and transduction, combined with a significantly reduced AAV dose.

MATERIALS AND METHODS

Animals

Experiments were conducted on 2–3 kg male (2–4 years old), captive-bred *cynomolgus macaque* purchased from BioPrim (Baziège, France) or from Silabe (Strasbourg, France) and housed in the Boisbonne Center at Nantes Veterinary School (Oniris, Nantes, France). The experiments were approved by the Regional Ethics Committee and were carried out according to European guidelines for the care and use of experimental animals (authorization number CEEA.2011.29). We selected primates that had no detectable or low titers (<1/50) of neutralizing factors against AAV serotypes 9 and 10 in the serum. All blood samples were collected under ketamine-induced anesthesia 10 mg/kg (Imalgene; Merial).

AAV Vectors

Vectors were generated by packaging AAV2-based recombinant genomes in AAV9 and AAVrh10 capsids by the helper virus-free transfection of HEK293 cells at the University Hospital of Nantes (<http://umr1089.univ-nantes.fr/>). The vectors were purified using an optimized cesium chloride gradient-based purification protocol, as previously described.²⁰ The AAV2 plasmids contain the gene encoding the GFP under the control of a ubiquitous hybrid of the CBA and 4 repeated sequences of miR142. Physical particles were quantified by dot blot hybridization, and vector titers are expressed as vector genomes per milliliter.

In Vivo AAV Injections

The animals were sedated with ketamine 10 mg/kg (Imalgene; Merial) and medetomidine 20 µg/kg, intubated, and anesthesia was continued by inhalation of 1% to 2% isoflurane in oxygen. Then, 1 to 1.5 mL of CSF was systematically removed before LIT-KT or ICV injection of AAV vectors. For LIT-KT administration, the animal was placed in lateral recumbence, and a catheter (pediatric epidural catheterization set, 25G + epidural needle 21G) was introduced via a SPROTTE cannula into the intrathecal space L3–L4. Placement was verified by the presence of CSF and real-time radioscopy examination. The catheter was slowly ascended to the cervical vertebrae under radioscopy control, and a solution of 1 mL of vector was then infused at a rate of 0.5 mL/min. The catheter was removed from 8 cm to be opposite of the thoracic vertebrae, and a new injection of 1 mL of vector was performed. The last deposit of 1 mL of vector occurred opposite of the first lumbar vertebrae and was followed by a flush of 0.4 mL of sterile saline. The needle was removed, and the animal was maintained in lateral recumbence for 1 h until recovery from anesthesia. The primates received 2.5E+13 vg of scAAVrh10-CBA-GFP or scAAV9-CBA-GFP.

For ICV administration, presurgical MRI was performed to establish brain coordinates. A small burr hole was made through the frontal bone, 20 mm caudally to the supraorbital arch and 2.5 mm laterally to the sagittal suture. A catheter (18G 1.3 × 32 mm) was introduced at a depth of 20 mm. The correct placement was verified by injecting 0.25 mL of contrast agent (Iopamiron; Bracco Imaging, France) under real-time radioscopy examination. Then, a solution of 0.5 mL of vector was infused at a rate of 0.1 mL/min, followed by a flush of 0.05 mL sterile saline. Primates received 4.5E+12 vg of scAAV9-CBA-GFP. A postsurgical MRI examination was performed to ensure the absence of neurologic lesions that could occur after ICV administration. The animal was then maintained in lateral recumbence until recovery from anesthesia. Throughout all surgical procedures, temperature, cardiac, respiratory frequency, capnography, pulse and electrocardiography were monitored.

The injected animals were immunosuppressed with sirolimus 2 mg/kg/day (Rapamune), prednisolone 1 to 2 mg/kg/day (Dermipred), and mycophenolate mofetil 40 mg/kg/day (CellCept) to avoid an immune response against AAV vectors and the transduced cells.

Clinical Follow-up

All injected primates were clinically evaluated before lumbar intrathecal or ICV injection and at 6 h and 1, 3, and 21 days thereafter. Animal behavior was evaluated using a video recording and a battery of cognitive, behavioral, neurological, and motor tests, following a protocol described by Ciron et al.²⁰ After becoming habituated with the experimenter for 10 min, posture, gait, movements, behavior in response to auditory and visual stimulation, and fine motility were examined. Reflexes, temperature, heart frequency, and skinfold were evaluated after sedation with ketamine 10 mg/kg (Imalgene; Merial).

Tissue Collection and Processing

3 weeks following vector delivery, the animals were anaesthetized (150 µg/kg medetomidine, 10 mg/kg ketamine, 0.2 mg/kg morphine, followed by 2% isoflurane inhalation), the spleen and inguinal lymph nodes were removed, and the animals were euthanized by a perfusion of 100 mL of PBS and 400 mL 4% paraformaldehyde (PFA) in the carotid. The brain was placed on a monkey coronal brain matrix (Pelco, Redding, CA) and cut into 2-mm-thick coronal sections. Even slabs were postfixed by incubation in 4% PFA, cryoprotected, frozen on dry ice, and cryostat sectioned (10 µm) for morphological and immunohistochemical studies. Individualized cerebral structures of odd slabs were snap frozen in liquid nitrogen and then stored at –80°C for vg detection. The spinal cord was removed and cut into coronal 5-mm blocks, postfixed by incubation in 4% PFA, and cryoprotected by overnight incubation in 30% sucrose. The samples were then embedded in optimal cutting temperature compound, frozen on dry ice, and cryostat sectioned (10 µm). For vg detection, the ventral and dorsal parts of the cervical, thoracic, and lumbar spinal cord and the left and right DRG of these regions were snap frozen in liquid nitrogen and then stored at –80°C. The muscles, cranial, and peripheral nerves, liver, spleen, heart, kidney, and testis were also collected both for vg detection and morphological studies.

Assessment of GFP Fluorescent Signal Specificity

The GFP signal was analyzed by using a spectral confocal microscope (LSM780; Karl Zeiss, Oberkochen, Germany). The Zeiss spectral system is able to record the fluorescence signals simultaneously every 9 nm on 34 separate detection channels, pixel by pixel, during scanning. With the use of this detection system, the autofluorescence signal was separated from the GFP fluorescence signal in the tissue. The autofluorescence spectrum was determined from the tissue sections of a noninjected NHP (negative control without GFP expression). The GFP spectrum was obtained from a GFP-positive cell of an AAV9-GFP-injected NHP with strong expression of GFP (positive control, Mac 3). By using autofluorescence, GFP reference spectra, and the Zeiss “Online Finger Printing” feature, the GFP fluorescence was separated from autofluorescence simultaneously during acquisition and as previously performed in our mice study.²⁴

Immunostaining and Motor Neuron Quantification

Spinal cord and brain slices were examined for GFP expression using a laser-scanning confocal microscope. For ChAT immunofluorescence, the brain and spinal cord sections were blocked by incubation with 1% rabbit serum (Dako, Les Ulis, France) in 0.4% Triton X-100 in PBS and incubated overnight at room temperature with a goat polyclonal anti-ChAT antibody (1:100; Chemicon International, Temecula, CA, USA); the sections were then incubated with a biotinylated rabbit anti-goat antibody (Dako). For NeuN, GFAP, Olig2, and Iba1 immunostaining, the brain and spinal cord sections were incubated overnight at room temperature with antibodies directed against GFAP (Dako), Olig2 (Millipore, Billerica, MA, USA), and Iba1 (Wako), followed by a biotinylated rabbit anti-goat antibody (Dako). The sections were then incubated with Alexa Fluor

555-conjugated streptavidin (Life Technologies, Saint Aubin, France), mounted in Mowiol (Calbiochem, San Diego, CA), and scanned serially using an argon ion laser (488 nm) to observe GFP signals and a helium neon laser (543 nm) to observe Alexa Fluor 555 signals. Each image was recorded in a separated channel (green channel for GFP and red channel for Alexa Fluor 555) and overlaid for the detection of colocalized fluorescent signals. For MN counts, three serial 25 μm cryosections per animal and per cervical, thoracic, and lumbar spinal cord samples per animals, separated by 50 μm , were immunolabeled for ChAT and counterstained using Nissl (NeuroTrace; Molecular Probes, Life Technologies). The proportion of ChAT/GFP double-positive cells relative to the total number of MNs in the ventral horn was determined for each section using Fiji freeware (<https://fiji.sc/>).

Muscle Fibers and Peripheral Organ GFP Expression and Quantification

The 10- μm -thick frozen-tissue sections (gastrocnemius, triceps brachii, diaphragm, heart, liver) were made by using cryostat (Leica). After 4% PFA fixation for 5 min and 3 \times 5-min successive PBS baths, the slides were mounted using Mowiol mounting medium and observed under the spectral confocal microscope LSM 780 (Zeiss). For the quantification of GFP in skeletal muscle, diaphragm, heart, and liver, the microscopic fields were randomly selected to evaluate at least 1,000 cells for each peripheral organ explored using 20 \times magnification. Fiji freeware (<https://fiji.sc/>) was used for cell counting and area measurements.

Quantitative PCR Analysis

To analyze the number of AAV particles in the serum and CSF of the injected animals, the genome of AAV was extracted from the serum and CSF before and at different times post-injection using a nucleospin RNA virus kit (Macherey Nagel, Düren, Germany). GFP-specific real-time PCR was conducted in duplicate with the Thermocycler StepOne Plus System (Applied Biosystem) using 10 μL of extracted viral DNA in a 25- μL final volume of the following solution: 12.5 μL Premix ExTaq (TaqMan Fast Universal PCR Master Mix), 0.5 μL 10 μM primer, 0.125 μL 10 μM 6-carboxyfluorescein/tetramethylrhodamine (FAM/TAMRA) TaqMan probe, and 1.38 μL H₂O. The cycle threshold (Ct) values were compared to those obtained with plasmid standard dilutions containing GFP cDNA sequences and a range of AAV particles mixed in the serum or CSF of noninjected NHPs. The primers and probes for GFP were as follows: forward primer 5'-ACTACAACAGCCACAACGTC TATATCA-3', reverse primer 5'-GGCGGATCTTGAAGTTC ACC-3', probe 6FAM5'-CCGACAAGCAGAAGAACGGCATCA-3'-TAMRA; and ϵ -globin: forward primer 5'-TGGCAAGGAGTTC ACCCCT-3', reverse primer 5'-AATGGCGACAGCAGACACC-3', probe 6FAM5'-TGCAGGCTGCCTGGCAGAAGC-3'-TAMRA. The samples were heated at 95°C for 20 s, followed by 40 cycles at 95°C for 3 s and 62°C for 30 s. Control tissues extracted separately from the vector-treated tissues were checked for GFP amplification. The sensitivity of the quantitative PCR is 10⁻³ copies/cell or 10 copies/50 ng of genomic DNA.

Detection of AAV9- and AAVrh10-Directed Neutralizing Factors

AAV9- and AAVrh10-directed NFs were assessed in primate serum before and at 3 weeks following vector injection, as previously described in Guilbaud et al.⁵¹ Briefly, human wild-type adenovirus type 5 was incubated on a rAAV-permissive cell line for 2 h. Recombinant AAV9 or AAVrh10 expressing the LacZ product was incubated with 10-fold dilutions of biologic fluids (serum or CSF) and then added to Ad5 preinfected cells. After incubation for 24 h at 37°C and 5% CO₂, the cells were fixed with 0.5% glutaraldehyde and then stained with X-Gal solution (Promega, Madison, WI, USA). The neutralizing factor titer was reported as the highest serum or CSF dilution that inhibited rAAV transduction (β -galactosidase expression) compared to the transduction control (rAAV without serum or CSF).

SUPPLEMENTAL INFORMATION

Supplemental Information can be found online at <https://doi.org/10.1016/j.omtm.2020.04.001>.

AUTHOR CONTRIBUTIONS

B.J. designed the study. B.J., J.D., J.H., and T.L. conducted the animal experiments. J.C. performed surgical injection procedures. J.-Y.D. conducted the veterinary care. M.F. provided MRI imaging expertise. L.D. provided bio-imaging expertise. J.D. performed histological analyses. C.C., M.L.B., K.M., M.M., R.M., and M.G. participated in the investigation. V.B. conducted the AAV production. O.A. conducted the immune-response analysis. K.B. performed data analysis. P.M., N.C., P.A., and M.-A.C. discussed the results. M.-A.C. conceived the project, was responsible for the research coordination and strategy, and is the guarantor of this work. K.B. and M.-A.C. wrote the manuscript.

CONFLICTS OF INTEREST

The authors declare no competing interests.

ACKNOWLEDGMENTS

We thank the staff of the Boisbonne Center for Gene Therapy (Oniris, Atlantic Gene Therapies, Nantes, France) for assistance with handling, care, surgical, and euthanasia procedures. We also thank the vector core, CPV (Centre de Production de Vecteurs; <http://umr1089.univ-nantes.fr/plateaux-technologiques/cpv/centre-de-production-de-vecteurs-2194757.kjsp?RH=1518531897125>) (INSERM U1089, Nantes, France), for the production of AAV vectors and Marie Devaux and Johanne Leduff from the Gene Therapy Immunology core (<https://umr1089.univ-nantes.fr/plateaux-technologiques/pac/>). This work was supported by a grant from Investissement d'Avenir (ANR-11-INBS-0011; NeurATRIS: A Translational Research Infrastructure for Biotherapies in Neurosciences), the Association Française contre les Myopathies (AFM), and the Région Pays de la Loire.

REFERENCES

1. Foust, K.D., Nurre, E., Montgomery, C.L., Hernandez, A., Chan, C.M., and Kaspar, B.K. (2009). Intravascular AAV9 preferentially targets neonatal neurons and adult astrocytes. *Nat. Biotechnol.* 27, 59–65.

2. Duque, S., Joussemet, B., Riviere, C., Marais, T., Dubreil, L., Douar, A.M., Fyfe, J., Moullier, P., Colle, M.A., and Barkats, M. (2009). Intravenous administration of self-complementary AAV9 enables transgene delivery to adult motor neurons. *Mol. Ther.* 17, 1187–1196.
3. Foust, K.D., Wang, X., McGovern, V.L., Braun, L., Bevan, A.K., Haidet, A.M., Le, T.T., Morales, P.R., Rich, M.M., Burghes, A.H., and Kaspar, B.K. (2010). Rescue of the spinal muscular atrophy phenotype in a mouse model by early postnatal delivery of SMN. *Nat. Biotechnol.* 28, 271–274.
4. Valori, C.F., Ning, K., Wyles, M., Mead, R.J., Grierson, A.J., Shaw, P.J., and Azzouz, M. (2010). Systemic Delivery of scAAV9 Expressing SMN Prolongs Survival in a Model of Spinal Muscular Atrophy. *Sci. Transl. Med.* 2, 35ra42.
5. Mendell, J.R., Al-Zaidy, S., Shell, R., Arnold, W.D., Rodino-Klapac, L.R., Prior, T.W., Lowes, L., Alfano, L., Berry, K., Church, K., et al. (2017). Single-Dose Gene-Replacement Therapy for Spinal Muscular Atrophy. *N. Engl. J. Med.* 377, 1713–1722.
6. Bevan, A.K., Duque, S., Foust, K.D., Morales, P.R., Braun, L., Schmelzer, L., Chan, C.M., McCrate, M., Chicoine, L.G., Coley, B.D., et al. (2011). Systemic gene delivery in large species for targeting spinal cord, brain, and peripheral tissues for pediatric disorders. *Mol. Ther.* 19, 1971–1980.
7. Nathwani, A.C., Tuddenham, E.G., Rangarajan, S., Rosales, C., McIntosh, J., Linch, D.C., Chowdhury, P., Riddell, A., Pie, A.J., Harrington, C., et al. (2011). Adenovirus-associated virus vector-mediated gene transfer in hemophilia B. *N. Engl. J. Med.* 365, 2357–2365.
8. Nathwani, A.C., Reiss, U.M., Tuddenham, E.G., Rosales, C., Chowdhury, P., McIntosh, J., Della Peruta, M., Lheriteau, E., Patel, N., Raj, D., et al. (2014). Long-term safety and efficacy of factor IX gene therapy in hemophilia B. *N. Engl. J. Med.* 371, 1994–2004.
9. Saal, K.-A., Koch, J.C., Tatenhorst, L., Szegő, E.M., Ribas, V.T., Michel, U., Bähr, M., Tönges, L., and Lingor, P. (2015). AAV.shRNA-mediated downregulation of ROCK2 attenuates degeneration of dopaminergic neurons in toxin-induced models of Parkinson's disease in vitro and in vivo. *Neurobiol. Dis.* 73, 150–162.
10. Ren, X., Zhang, T., Gong, X., Hu, G., Ding, W., and Wang, X. (2013). AAV2-mediated striatum delivery of human CDNF prevents the deterioration of midbrain dopamine neurons in a 6-hydroxydopamine induced parkinsonian rat model. *Exp. Neurol.* 248, 148–156.
11. Oh, S.-M., Chang, M.Y., Song, J.J., Rhee, Y.H., Joe, E.H., Lee, H.S., Yi, S.H., and Lee, S.H. (2015). Combined Nurr1 and Foxa2 roles in the therapy of Parkinson's disease. *EMBO Mol. Med.* 7, 510–525.
12. Herzog, C.D., Brown, L., Kruegel, B.R., Wilson, A., Tansey, M.G., Gage, F.H., Johnson, E.M., Jr., and Bartus, R.T. (2013). Enhanced neurotrophic distribution, cell signaling and neuroprotection following substantia nigral versus striatal delivery of AAV2-NRTN (CERE-120). *Neurobiol. Dis.* 58, 38–48.
13. Rocha, E.M., Smith, G.A., Park, E., Cao, H., Brown, E., Hayes, M.A., Beagan, J., McLean, J.R., Izen, S.C., Perez-Torres, E., et al. (2015). Glucocerebrosidase gene therapy prevents α -synucleinopathy of midbrain dopamine neurons. *Neurobiol. Dis.* 82, 495–503.
14. Sevin, C., Benraiss, A., Van Dam, D., Bonnin, D., Nagels, G., Verot, L., Laurendeau, I., Vidaud, M., Gieselmann, V., Vanier, M., et al. (2006). Intracerebral adeno-associated virus-mediated gene transfer in rapidly progressive forms of metachromatic leukodystrophy. *Hum. Mol. Genet.* 15, 53–64.
15. Ciron, C., Desmaris, N., Colle, M.A., Raoul, S., Joussemet, B., Vérot, L., Ausseil, J., Froissart, R., Roux, F., Chérel, Y., et al. (2006). Gene therapy of the brain in the dog model of Hurler's syndrome. *Ann. Neurol.* 60, 204–213.
16. Ellinwood, N.M., Ausseil, J., Desmaris, N., Bigou, S., Liu, S., Jens, J.K., Snella, E.M., Mohammed, E.E., Thomson, C.B., Raoul, S., et al. (2011). Safe, efficient, and reproducible gene therapy of the brain in the dog models of Sanfilippo and Hurler syndromes. *Mol. Ther.* 19, 251–259.
17. Hocquemiller, M., Giersch, L., Audrain, M., Parker, S., and Cartier, N. (2016). Adeno-Associated Virus-Based Gene Therapy for CNS Diseases. *Hum. Gene Ther.* 27, 478–496.
18. Tardieu, M., Zérah, M., Husson, B., de Bournonville, S., Deiva, K., Adamsbaum, C., Vincent, F., Hocquemiller, M., Broissand, C., Furlan, V., et al. (2014). Intracerebral administration of adeno-associated viral vector serotype rh.10 carrying human *SGSH* and *SUMF1* cDNAs in children with mucopolysaccharidosis type IIIA disease: results of a phase I/II trial. *Hum. Gene Ther.* 25, 506–516.
19. Tardieu, M., Zérah, M., Gougeon, M.L., Ausseil, J., de Bournonville, S., Husson, B., Zafeiriou, D., Parenti, G., Bourget, P., Poirier, B., et al. (2017). Intracerebral gene therapy in children with mucopolysaccharidosis type IIIB syndrome: an uncontrolled phase 1/2 clinical trial. *Lancet Neurol.* 16, 712–720.
20. Ciron, C., Cressant, A., Roux, F., Raoul, S., Chérel, Y., Hantraye, P., Déglon, N., Schwartz, B., Barkats, M., Heard, J.M., et al. (2009). Human α -iduronidase gene transfer mediated by adeno-associated virus types 1, 2, and 5 in the brain of nonhuman primates: vector diffusion and biodistribution. *Hum. Gene Ther.* 20, 350–360.
21. Federici, T., Taub, J.S., Baum, G.R., Gray, S.J., Grieger, J.C., Matthews, K.A., Handy, C.R., Passini, M.A., Samulski, R.J., and Boulis, N.M. (2012). Robust spinal motor neuron transduction following intrathecal delivery of AAV9 in pigs. *Gene Ther.* 19, 852–859.
22. Gray, S.J., Nagabhusan Kalburgi, S., McCown, T.J., and Jude Samulski, R. (2013). Global CNS gene delivery and evasion of anti-AAV-neutralizing antibodies by intrathecal AAV administration in non-human primates. *Gene Ther.* 20, 450–459.
23. Samaranch, L., Sebastian, W.S., Kells, A.P., Salegio, E.A., Heller, G., Bringas, J.R., Pivrotto, P., DeArmond, S., Forsayeth, J., and Bankiewicz, K.S. (2014). AAV9-mediated expression of a non-self protein in nonhuman primate central nervous system triggers widespread neuroinflammation driven by antigen-presenting cell transduction. *Mol. Ther.* 22, 329–337.
24. Bey, K., Ciron, C., Dubreil, L., Deniaud, J., Ledevin, M., Cristini, J., Blouin, V., Aubourg, P., and Colle, M.A. (2017). Efficient CNS targeting in adult mice by intrathecal infusion of single-stranded AAV9-GFP for gene therapy of neurological disorders. *Gene Ther.* 24, 325–332.
25. Hinderer, C., Bell, P., Katz, N., Vite, C.H., Louboutin, J.P., Bote, E., Yu, H., Zhu, Y., Casal, M.L., Bagel, J., et al. (2018). Evaluation of Intrathecal Routes of Administration for Adeno-Associated Viral Vectors in Large Animals. *Hum. Gene Ther.* 29, 15–24.
26. Swain, G.P., Prociuk, M., Bagel, J.H., O'Donnell, P., Berger, K., Drobatz, K., Gurda, B.L., Haskins, M.E., Sands, M.S., and Vite, C.H. (2014). Adeno-associated virus serotypes 9 and rh10 mediate strong neuronal transduction of the dog brain. *Gene Ther.* 21, 28–36.
27. Cearley, C.N., and Wolfe, J.H. (2006). Transduction characteristics of adeno-associated virus vectors expressing cap serotypes 7, 8, 9, and Rh10 in the mouse brain. *Mol. Ther.* 13, 528–537.
28. Bucher, T., Colle, M.A., Wakeling, E., Dubreil, L., Fyfe, J., Briot-Nivard, D., Mauguéneau, M., Raoul, S., Chérel, Y., Astord, S., et al. (2013). scAAV9 intracisternal delivery results in efficient gene transfer to the central nervous system of a feline model of motor neuron disease. *Hum. Gene Ther.* 24, 670–682.
29. Haurigot, V., Marcó, S., Ribera, A., Garcia, M., Ruzo, A., Villacampa, P., Ayuso, E., Añor, S., Andaluz, A., Pineda, M., et al. (2013). Whole body correction of mucopolysaccharidosis IIIA by intracerebrospinal fluid gene therapy. *J. Clin. Invest.* 123, 3254–3271.
30. Hordeaux, J., Dubreil, L., Robveille, C., Deniaud, J., Pascal, Q., Dequéant, B., Pailloux, J., Lagalice, L., Ledevin, M., Babarit, C., et al. (2017). Long-term neurologic and cardiac correction by intrathecal gene therapy in Pompe disease. *Acta Neuropathol. Commun.* 5, 66.
31. Hinderer, C., Bell, P., Vite, C.H., Louboutin, J.P., Grant, R., Bote, E., Yu, H., Pukenas, B., Hurst, R., and Wilson, J.M. (2014). Widespread gene transfer in the central nervous system of cynomolgus macaques following delivery of AAV9 into the cisterna magna. *Mol. Ther. Methods Clin. Dev.* 1, 14051.
32. Samaranch, L., Salegio, E.A., San Sebastian, W., Kells, A.P., Bringas, J.R., Forsayeth, J., and Bankiewicz, K.S. (2013). Strong cortical and spinal cord transduction after AAV7 and AAV9 delivery into the cerebrospinal fluid of nonhuman primates. *Hum. Gene Ther.* 24, 526–532.
33. Pilon, R.N., and Baker, A.R. (1976). Chronic pain control by means of an epidural catheter: report of a case with description of the method. *Cancer* 37, 903–905.
34. Sprotte, G. (1995). [An atraumatic needle for continuous epidural and plexus anesthesia]. *Anaesthetist* 44, 789–792.
35. Rangel-Castillo, L., Gopinath, S., and Robertson, C.S. (2008). Management of Intracranial Hypertension. *Neurol. Clin.* 26, 521–541.
36. Zieglgänsberger, W. (2019). Substance P and pain chronicity. *Cell Tissue Res.* 375, 227–241.

37. Hinderer, C., Katz, N., Buza, E.L., Dyer, C., Goode, T., Bell, P., Richman, L.K., and Wilson, J.M. (2018). Severe Toxicity in Nonhuman Primates and Piglets Following High-Dose Intravenous Administration of an Adeno-Associated Virus Vector Expressing Human SMN. *Hum. Gene Ther.* 29, 285–298.
38. Hordeaux, J., Hinderer, C., Goode, T., Buza, E.L., Bell, P., Calcedo, R., Richman, L.K., and Wilson, J.M. (2018). Toxicology Study of Intra-Cisterna Magna Adeno-Associated Virus 9 Expressing Iduronate-2-Sulfatase in Rhesus Macaques. *Mol. Ther. Methods Clin. Dev.* 10, 68–78.
39. Schuster, D.J., Dykstra, J.A., Riedl, M.S., Kitto, K.F., Belur, L.R., McIvor, R.S., Elde, R.P., Fairbanks, C.A., and Vulchanova, L. (2014). Biodistribution of adeno-associated virus serotype 9 (AAV9) vector after intrathecal and intravenous delivery in mouse. *Front. Neuroanat.* 8, 42.
40. Schwarz, S., Georgiadis, D., Aschoff, A., and Schwab, S. (2002). Effects of body position on intracranial pressure and cerebral perfusion in patients with large hemispheric stroke. *Stroke* 33, 497–501.
41. Wang, H., Yang, B., Qiu, L., Yang, C., Kramer, J., Su, Q., Guo, Y., Brown, R.H., Jr., Gao, G., and Xu, Z. (2014). Widespread spinal cord transduction by intrathecal injection of rAAV delivers efficacious RNAi therapy for amyotrophic lateral sclerosis. *Hum. Mol. Genet.* 23, 668–681.
42. Borel, F., Gernoux, G., Sun, H., Stock, R., Blackwood, M., Brown, R.H., Jr., and Mueller, C. (2018). Safe and effective superoxide dismutase 1 silencing using artificial microRNA in macaques. *Sci. Transl. Med.* 10, eaau6414.
43. Samaranch, L., Salegio, E.A., San Sebastian, W., Kells, A.P., Foust, K.D., Bringas, J.R., Lamarre, C., Forsayeth, J., Kaspar, B.K., and Bankiewicz, K.S. (2012). Adeno-associated virus serotype 9 transduction in the central nervous system of nonhuman primates. *Hum. Gene Ther.* 23, 382–389.
44. Matsuzaki, Y., Konno, A., Mukai, R., Honda, F., Hirato, M., Yoshimoto, Y., and Hirai, H. (2017). Transduction Profile of the Marmoset Central Nervous System Using Adeno-Associated Virus Serotype 9 Vectors. *Mol. Neurobiol.* 54, 1745–1758.
45. Iliff, J.J., Wang, M., Liao, Y., Plogg, B.A., Peng, W., Gundersen, G.A., Benveniste, H., Vates, G.E., Deane, R., Goldman, S.A., et al. (2012). A Paravascular Pathway Facilitates CSF Flow Through the Brain Parenchyma and the Clearance of Interstitial Solutes, Including Amyloid β . *Sci. Transl. Med.* 4, 147ra111.
46. Meyer, K., Ferraiuolo, L., Schmelzer, L., Braun, L., McGovern, V., Likhite, S., Michels, O., Govoni, A., Fitzgerald, J., Morales, P., et al. (2015). Improving single injection CSF delivery of AAV9-mediated gene therapy for SMA: a dose-response study in mice and nonhuman primates. *Mol. Ther.* 23, 477–487.
47. Vulchanova, L., Schuster, D.J., Belur, L.R., Riedl, M.S., Podetz-Pedersen, K.M., Kitto, K.F., Wilcox, G.L., McIvor, R.S., and Fairbanks, C.A. (2010). Differential Adeno-Associated Virus Mediated Gene Transfer to Sensory Neurons following Intrathecal Delivery by Direct Lumbar Puncture. *Mol. Pain* 6, 31.
48. Sakka, L., Coll, G., and Chazal, J. (2011). Anatomy and physiology of cerebrospinal fluid. *Eur. Ann. Otorhinolaryngol. Head Neck Dis.* 128, 309–316.
49. Castle, M.J., Perlson, E., Holzbaur, E.L., and Wolfe, J.H. (2014). Long-distance axonal transport of AAV9 is driven by dynein and kinesin-2 and is trafficked in a highly motile Rab7-positive compartment. *Mol. Ther.* 22, 554–566.
50. Green, F., Samaranch, L., Zhang, H.S., Manning-Bog, A., Meyer, K., Forsayeth, J., and Bankiewicz, K.S. (2016). Axonal transport of AAV9 in nonhuman primate brain. *Gene Ther.* 23, 520–526.
51. Guilbaud, M., Devaux, M., Couzinié, C., Le Duff, J., Toromanoff, A., Vandamme, C., Jaulin, N., Gernoux, G., Larcher, T., Moullier, P., et al. (2019). Five Years of Successful Inducible Transgene Expression Following Locoregional Adeno-Associated Virus Delivery in Nonhuman Primates with No Detectable Immunity. *Hum. Gene Ther.* 30, 802–813.

Supplemental Information

Intra-CSF AAV9 and AAVrh10 Administration in Nonhuman Primates: Promising Routes and Vectors for Which Neurological Diseases?

Karim Bey, Johan Deniaud, Laurence Dubreil, Béatrice Joussemet, Joseph Cristini, Carine Ciron, Juliette Hordeaux, Morwenn Le Boulc'h, Kevin Marche, Maud Maquigneau, Michaël Guilbaud, Rosalie Moreau, Thibaut Larcher, Jack-Yves Deschamps, Marion Fusellier, Véronique Blouin, Caroline Sevin, Nathalie Cartier, Oumeya Adjali, Patrick Aubourg, Philippe Moullier, and Marie-Anne Colle

1 Supplemental Information

2

3 *Video S1: ICV contrast solution administration into right lateral ventricle in NHPs.*

4

5 *Figure S1: Focus on the ventral horns of thoracic and lumbar spinal cord of AAV-injected NHPs.*

6 Longitudinal section of the thoracic **(A)** and lumbar **(B)** spinal cord of Mac 3 NHP injected with AAV9-GFP by LIT-

7 KT injection demonstrating GFP expression across 5 mm. Scale bar = 1 mm. White hatched window into left panels

8 picture represents the focus of the ventral horn presented into the right panels. Scale bar = 150 μ m.

9

10 *Figure S2: Transduced-cell type identification throughout spinal cord following AAV9 intra-CSF delivery.*

11 AAV9 cell-specific tropism was determined in brain representative sections from NHPs injected by LIT-KT and ICV.

12 Brain tissues were immunolabelled using Olig 2, GFAP, Iba1 and NeuN primaries for oligodendrocytes, astrocytes,

13 microglial cells and neuron phenotyping, respectively, and an Alexa 555 (red channel)-coupled secondary antibody

14 was used for cell detection. GFP was determined by native GFP fluorescence signal imaging (green channel). Main

15 images show Alexa 555/GFP merged fluorescence signals. Scale bar = 100 μ m. Hatched windows indicate regions

16 with GFP-positive cells, and insets show higher magnification on cells harbouring both fluorescence signals: Alexa

17 555 (left) and GFP (right) channels. Scale bar = 25 μ m.

18

19 *Figure S3: Assessment of GFP specificity in NHP spinal cord and GFP-positive motor neurons quantification.*

20 Confocal microscopy spectral images of the monkey ventral horn spinal cord were taken to determine the

21 autofluorescence and native GFP fluorescence signal in the NHP spinal cord by using linear unmixing to separate

22 native GFP spectra from autofluorescence spectra. To demonstrate the specificity with which GFP fluorescence

23 is distinguished from autofluorescence, spectral imaging analysis was performed in **(A)** Mac 3 monkeys that

24 received scAAV9-CBA-GFP. **(B)** The autofluorescence spectrum was determined by analysis of PBS-injected

25 monkeys. Scale bar = 50 μ m. **(C)** Graphical representation of the spectrum profile of the autofluorescence signal

26 spectrum (**○**) and native GFP spectrum (**■**) demonstrating distinct emission wavelengths. **(D)** Quantification of

27 ChAT/GFP colocalization in MN in cervical, thoracic and lumbar spinal cord of each NHP used in the study.

28

29 *Figure S4: Brain analysed sections and GFP expression mapping.*

30 **(A)** Representative macroscopic dissection of the NHP brain included in the study. GFP expression mapping was

31 performed in right hemisphere coronal sections 4, 16 and 23. Adapted from Colle et al. [10] **(B)** In coronal section 4,
32 25- μ m cryosection was performed, and GFP expression was analysed by confocal microscopy in the frontal cortex
33 (inset). In coronal section 16, GFP expression was analysed in the parietal cortex (inset 5), temporal cortex (inset 2),
34 hippocampus (inset 1), body of caudate nucleus (inset 3), and putamen (inset 4). In coronal section 23, GFP expression
35 was analysed in the fourth ventricle area of the brain stem (inset 1) and in the cerebellum (inset 2). Scale bar = 150 μ m.
36

37 *Figure S5: Histopathological examination of the cervical, thoracic and lumbar DRGs.*

38 Haematoxylin, eosine and saffron staining were performed in cervical, thoracic and lumbar DRGs of all NHPs
39 included in the study. Photomicrographs presented in the figure demonstrate representative histopathological lesions
40 found in AAVrh10- and AAV9-LIT-KT-injected monkeys. Black arrows show mononuclear cell infiltration and black
41 arrowhead point myelin digestion chambers in DRGs. Scale bar = 150 μ m.
42

43 *Figure S6: GFP expression in peripheral organs*

44 GFP expression in peripheral organs following AAVrh10- and AAV9-LIT-KT and AAV9-ICV injection in NHP.
45 Peripheral tissues were counter stained with 4',6-diamidino-2-phenylindole (DAPI) and native GFP expression
46 was microscopically evaluated in the thymus, the spleen, the lung, the kidney, the jejunum and the testis. Scale
47 bar = 150 μ m (thymus – jejunum) and 50 μ m (testis). White hatched windows represent the focus in one region of
48 interest, presented into the left panels of each main photomicrograph. Scale bar = 50 μ m (thymus – jejunum) and 10
49 μ m.
50

51 *Figure S7: GFP is expressed surrounding the Virchow-Robin space.*

52 Representative confocal imaging was performed in injected NHPs brain 25- μ m cryosection for the identification of the
53 Virchow-Robin perivascular space and GFP expression in that same area. Endothelial cells and GFP are demonstrated
54 by using red channels and green channels, respectively. Lumens of vessels are demonstrated by asterisks. Scale bar =
55 100 μ m.
56

57

58

59

60

61

61 *Table S1: Cellular and humoral immune responses against the GFP transgene.*

62
63
64
65
66
67
68
69
70
71

<i>Animal identification</i>	<i>Route</i>	<i>Capsid</i>	<i>IFN γ ELISPOT *^a</i>		<i>Anti-GFP IgG antibodies</i>			
			<i>PBMC</i>	<i>Splenocytes</i>	<i>d3</i>	<i>d7</i>	<i>d10</i>	<i>d Euth</i>
Mac 1	IT	10	+	+	NA	NA	NA	1/20480
Mac 2	IT	10	-	-	nd	nd	nd	nd
Mac 3	IT	9	+	-	nd	nd	nd	1/2560
Mac 4	IT	9	+	+	nd	nd	nd	1/2560
Mac 5	IT	9	-	-	nd	nd	nd	nd
Mac 6	IT	9	-	-	nd	nd	nd	1/163840
Mac 7	ICV	9	-	+	nd	nd	nd	nd
Mac 8	ICV	9	-	+	nd	nd	nd	nd

* GFP peptid pools; ^a: ELISPOT was performed at euthanasia time point; d: day; +: positive responder to GFP peptide pools
- : negative responder to GFP peptide pools; NA: not available sample; nd: not determine

72
73
74
75
76
77
78
79
80
81
82
83

84 Figure S1

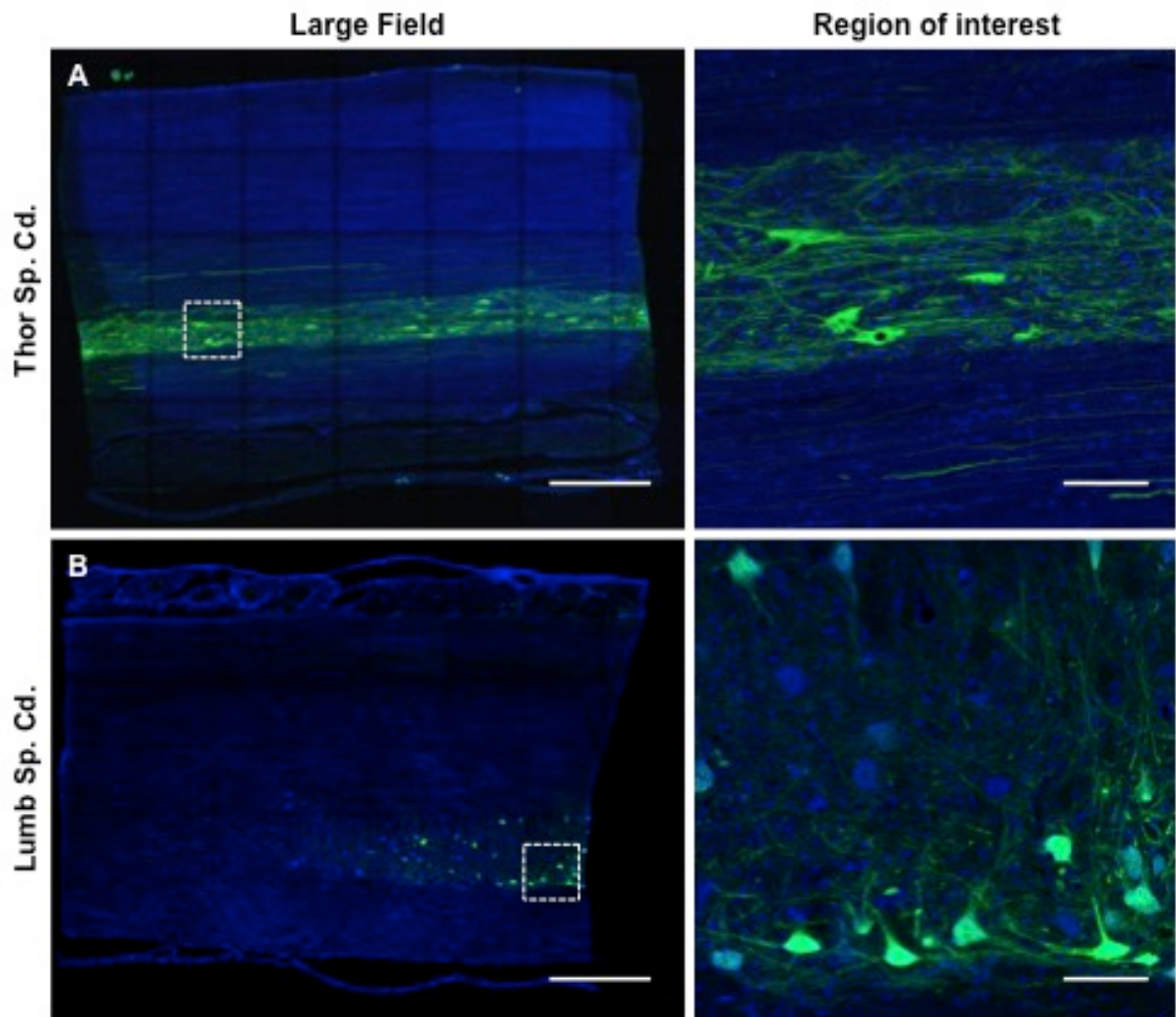
85

86

87

88

89



90

91

92

93

94

95

96

97 Figure S2

98

99

100

101

102

103

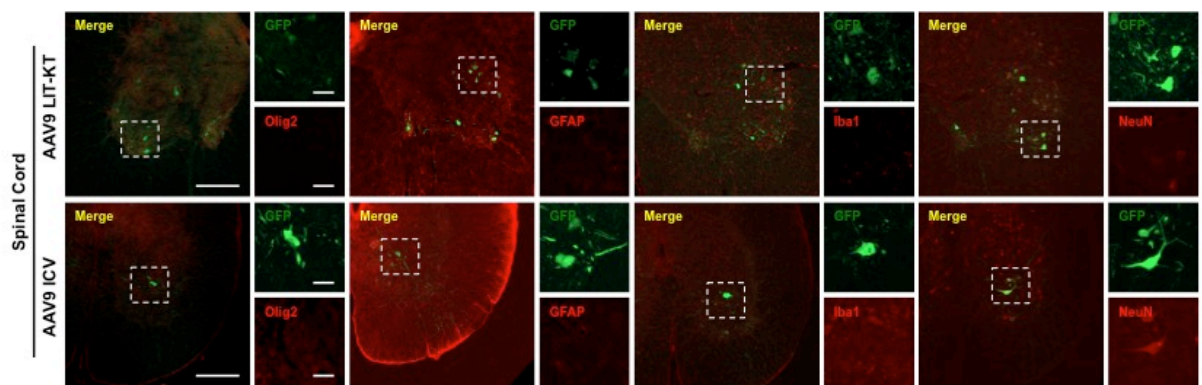
104

105

106

107

108



109

110

111

112

113

114

115

116

117

118

119

120

121 Figure S3

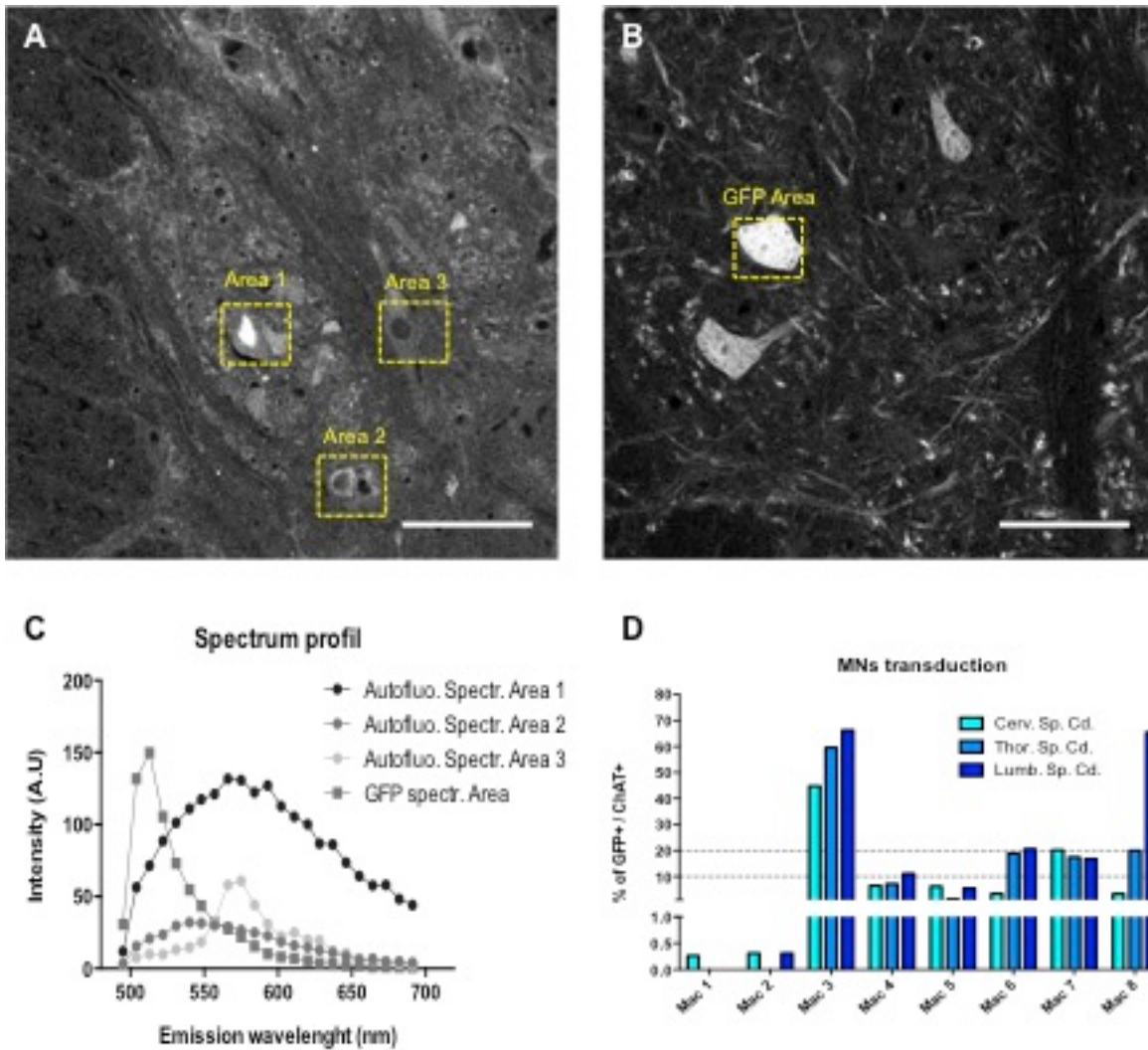
122

123

124

125

126



127

128

129

130

131

132

133 Figure S4

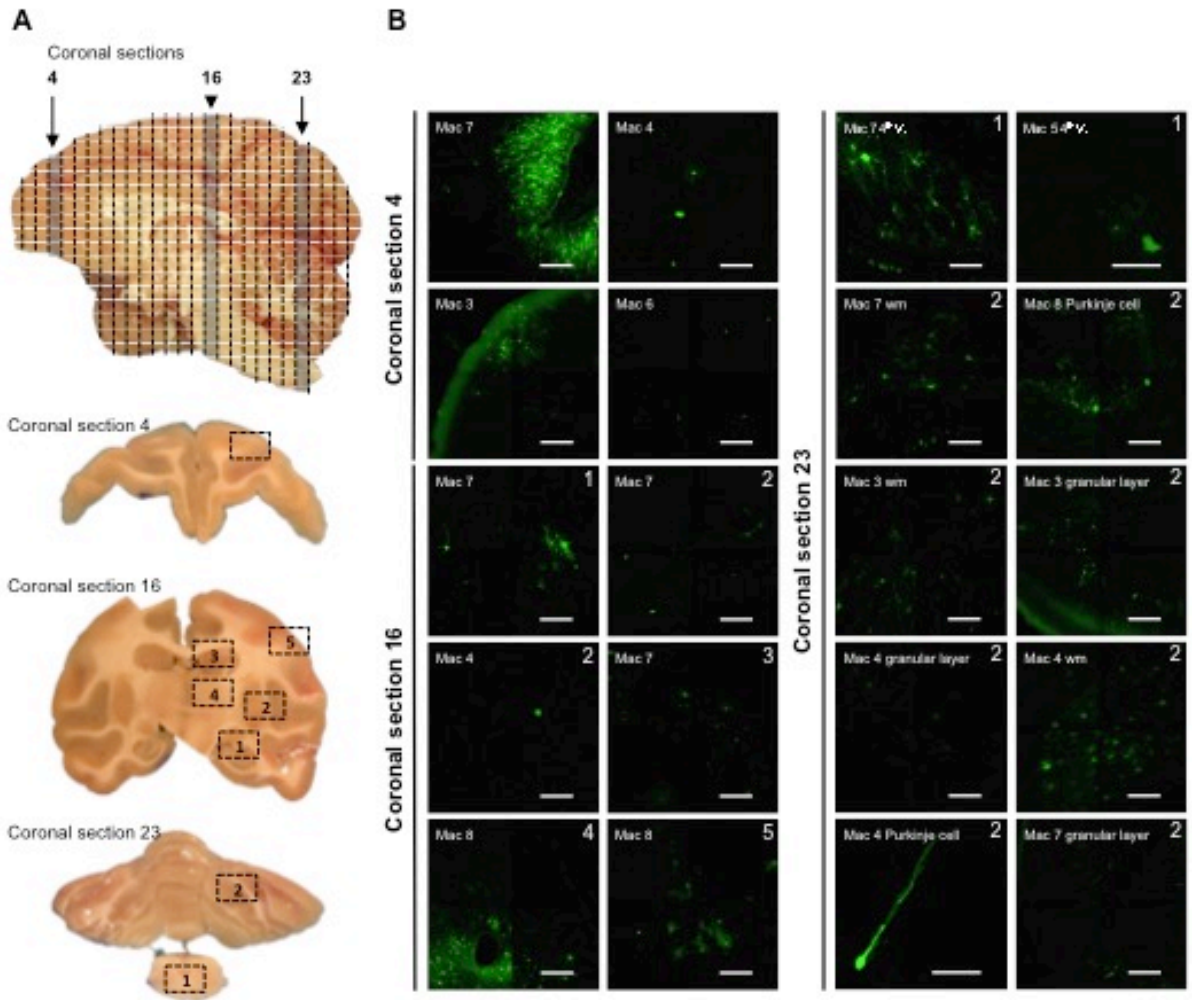
134

135

136

137

138



139

140

141

142

143

144

145

146 Figure S5

147

148

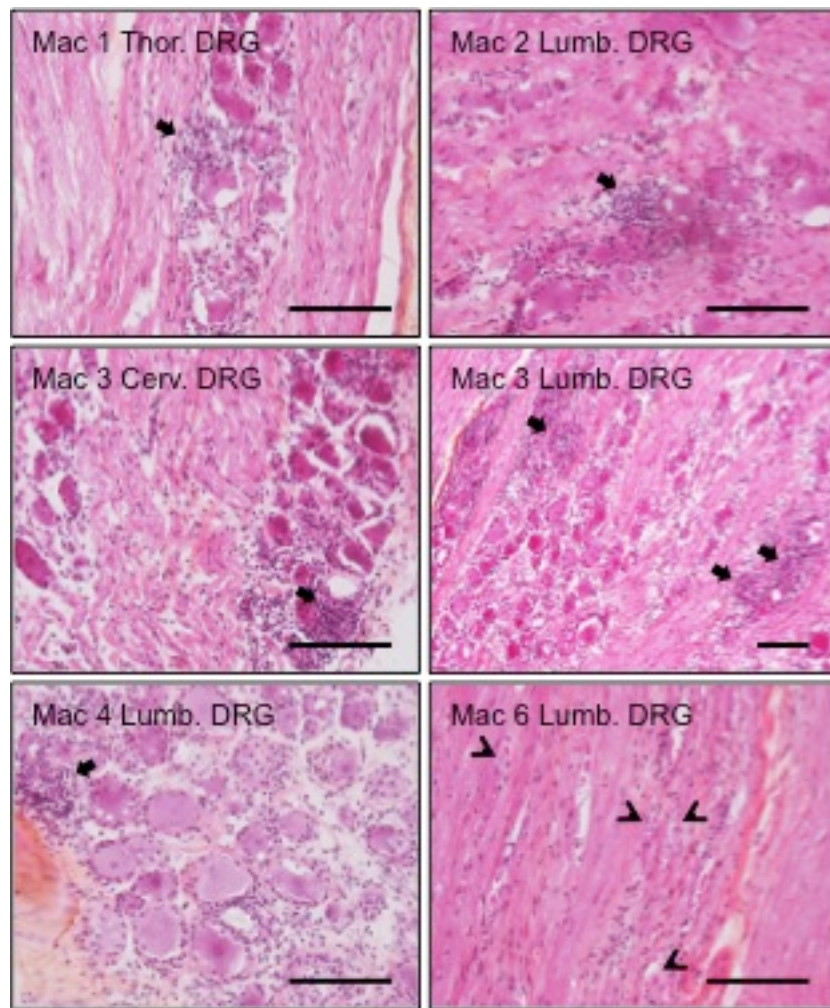
149

150

151

152

153



177

178

179

180

181

182

183

184

185

186

187

188

189

190

191

192

193

194

195

196

197

198

199

200

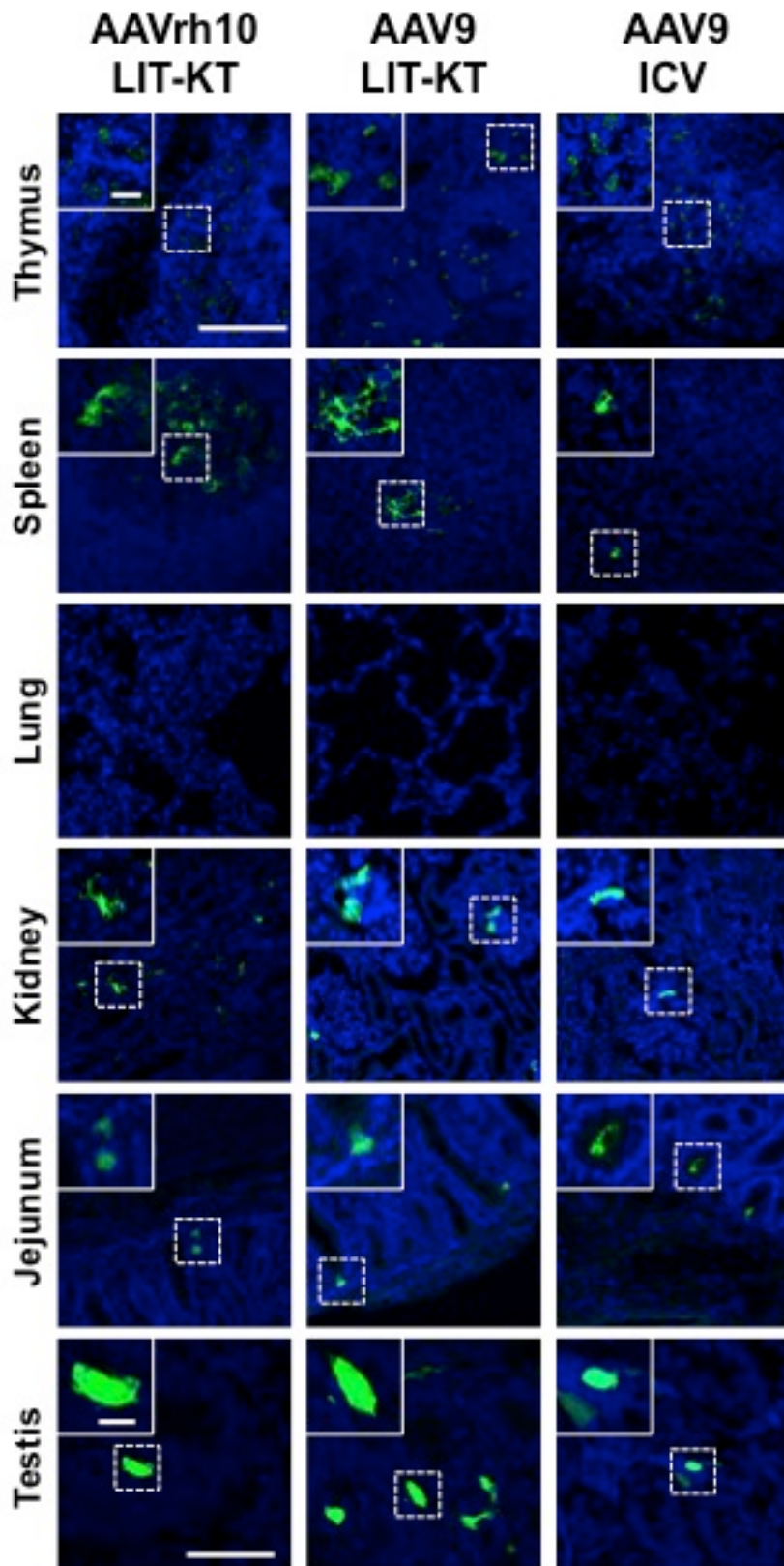
201

202

203

204

205



206 Figure S7

207

208

209

210

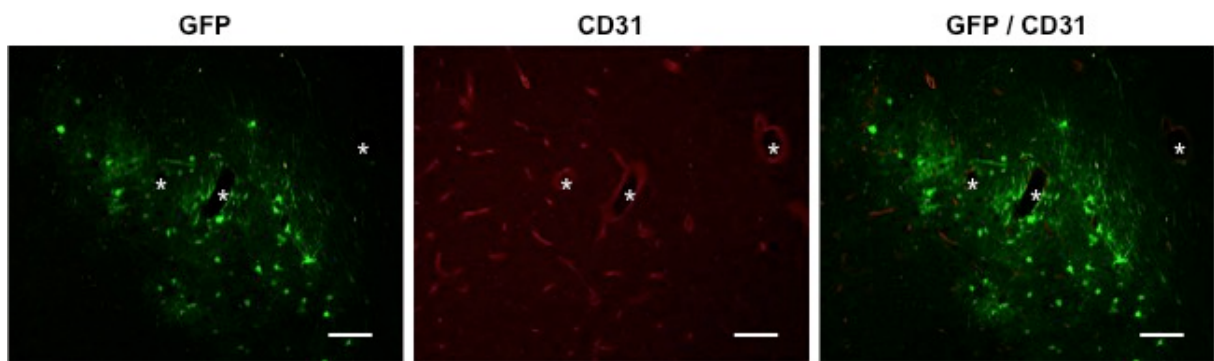
211

212

213

214

215



216 Video S1
217
218
219
220



221
222
223
224
225

226 **Supplemental Methods**

227

228 *Detection of anti-transgene humoral response*

229 The presence of anti-GFP antibodies in primate sera was assessed by enzyme-linked immunosorbent assay
230 (ELISA). Briefly, Nunc Maxisorp P96 plate (Thermo) was coated with 5 µg / mL of recombinant GFP protein
231 (Merck). After an overnight incubation at + 4 °C, the wells were washed, saturated and incubated with two-fold
232 dilutions of serum from 1/10 to 1/327,680. After 2 hours at 37 °C and a washing step, the wells were incubated
233 for 1 hour at 37 °C with horseradish peroxidase (HRP)-conjugated anti-Rhesus immunoglobulin G (IgG,
234 Southern Biotech). Signals were revealed using 2,2-3,3',5,5'-tetramethylbenzidine (TMB, Becton Dickinson)
235 according to the manufacturer's recommendations. Absorbance was read at 450 nm with a correction at 570 nm
236 on a Multiskan Go reader (Thermo). Threshold positivity was established from the mean of the optical density
237 obtained for each dilution + 2SD from 22 negative sera obtained from naïve primates. IgG titers for experimental
238 animals were defined as the highest serum dilution with an optical density that remained above the threshold.

239

240 *Detection of the anti-transgene cellular response by using an interferon gamma (IFN-γ) enzyme-linked*
241 *immunospot assay (ELISpot)*

242 Briefly, peripheral blood mononuclear cells (PBMCs) collected at euthanasia were thawed and dispatched at
243 2E+5 cells into human anti-IFN-γ (MabTech) precoated polyvinylidene difluoride membrane Multiscreen® high
244 throughput filter plates (Millipore). PBMCs were incubated with 5 peptide pools covering the GFP sequence
245 (overlapping peptide library 15 per 10 mers; Sigma-Aldrich). Pools were replaced by culture medium alone for
246 negative control or Concanavalin A for positive control. After 48 h of incubation at 37 °C in 5 % CO₂, the wells
247 were washed and incubated with a biotinylated anti-IFN-γ antibody (clone 7-B6-1) MabTech and then with
248 ExtrAvidin® alkaline phosphatase (Sigma Aldrich). The reaction was revealed using BCIP/NBT substrate
249 (Thermo), spots were counted using an ELISpot Reader ELR07 (AID) and analysed with the AID ELISpot
250 reader software v7.0. Only responses at least threefold higher than the negative control and above 50 spot-
251 forming colonies per million cells were considered positive.